Inorganic Chemistry

pubs.acs.org/IC Article

Oxygen Atom Transfer Reactivity of Molybdenum(VI) Complexes Employing Pyrimidine- and Pyridine-2-thiolate Ligands

Madeleine A. Ehweiner, Fabian Wiedemaier, Ferdinand Belaj, and Nadia C. Mösch-Zanetti*

Cite This: https://dx.doi.org/10.1021/acs.inorgchem.0c02412 Read Online

ABSTRACT: Four dioxidomolybdenum(VI) complexes of the general structure [MoO_2L_2] employing the S,N-bidentate ligands pyrimidine-2-thiolate (PymS, **1**), pyridine-2-thiolate (PyS, **2**), 4-methylpyridine-2-thiolate (4-MePyS, **3**) and 6-methylpyridine-2-thiolate (6-MePyS, **4**) were synthesized and characterized by spectroscopic means and single-crystal X-ray diffraction analysis (**2**−**4**). Complexes **1**−**4** were reacted with PPh_3 and PMe_3, respectively, to investigate their oxygen atom transfer (OAT) reactivity and catalytic applicability. Reduction with PPh_3 leads to symmetric molybdenum(V) dimers of the general structure [$Mo_2O_3L_4$] (**6**−**9**). Kinetic studies showed that the OAT from [MoO_2L_2] to PPh_3 is 5 times faster for the PymS system than for the PyS and 4-MePyS systems. The reaction of complexes **1**−**3** with PMe_3 gives stable molybdenum(IV) complexes of the structure [$MoOL_2(PMe_3)_2$] (**10**−**12**), while reduction of [MoO_2(6-MePyS)$_2$] (**4**) yields [MoO(6-MePyS)$_2$(PMe_3)] (**13**) with only one PMe_3 coordinated to the metal center. The activity of complexes **1**−**4** in catalytic OAT reactions involving Me_2SO and Ph_2SO as oxygen donors and PPh_3 as an oxygen acceptor has been investigated to assess the influence of the varied ligand frameworks on the OAT reaction rates. It was found that [MoO_2(PymS)$_2$] (**1**) and [MoO_2(6-MePyS)$_2$] (**4**) are similarly efficient catalysts, while complexes **2** and **3** are only moderately active. In the catalytic oxidation of PMe_3 with Me_2SO, complex **4** is the only efficient catalyst. Complexes **1**−**4** were also found to catalytically reduce NO_3^- with PPh_3, although their reactivity is inhibited by further reduced species such as NO, as exemplified by the formation of the nitrosyl complex [Mo(NO)(PymS)$_3$] (**14**), which was identified by single-crystal X-ray diffraction analysis. Computed $\Delta G^{\ddagger}$ values for the very first step of the OAT were found to be lower for complexes **1** and **4** than for **2** and **3**, explaining the difference in catalytic reactivity between the two pairs and revealing the requirement for an electron-deficient ligand system.

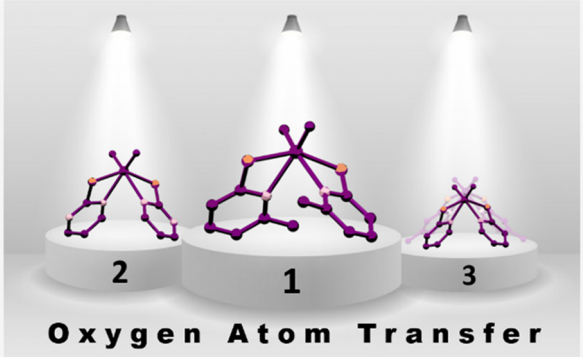

■ INTRODUCTION

Molybdenum is the only second-row transition metal that is required by most living organisms, where it is found as a mononuclear metal center in the active site of many enzymes.[1,2] With the exception of nitrogenase and related proteins, the active site of all molybdoenzymes contains a pyranopterin-dithiolene cofactor in which the metal is coordinated by the dithiolene moiety.[3−6] The dimethyl sulfoxide reductase (DMSOR) superfamily is structurally and catalytically the largest and most diverse family of molybdoenzymes, and reactions catalyzed by its members frequently involve oxygen atom transfer (OAT).[7−11] With these naturally occurring systems as inspiration, dioxidomolybdenum(VI) complexes have been extensively investigated in catalytic OAT reactions.[12−19] Since an aqueous environment has not been feasible for the majority of those complexes, a widespread model reaction, which was developed in the 1980s, is the OAT from Me_2SO to PPh_3, yielding Me_2S and $POPh_3$.[20−22] The ligands utilized in this model reaction are either dithiolene or non-dithiolene type systems.[23,24] Although bidentate non-dithiolene ligands with S,N, O,O, or N,O donor sets are structurally obviously different from the molybdopterin cofactor present in molybdoenzymes, they were found to be generally more suitable for molybdenum-catalyzed OAT reactions.[25−32] Even more different tri- and tetradentate ligands with various donor sets[33−40] have been successfully utilized, with the class of scorpionate ligands being outstanding.[41−48] Furthermore, various theoretical studies have been performed to assess the influence of the protein ligand[49,50] or charge differences[51] and to compare active sites containing either molybdenum or tungsten.[52,53] Apart from sulfoxides, molybdenum complexes could also be applied in the deoxygenation of more challenging substrates: nitrate is reduced by naturally occurring nitrate reductases belonging to

Received: August 12, 2020

the DMSOR superfamily and containing molybdenum in their active site.[7] However, artificial systems capable of reducing nitrate to nitrite remain scarce,[54−57] although nitrate contamination in groundwater associated with the excessive use of fertilizers and global industrialization is an increasing problem.[58,59] Thus, the development of efficient catalytic systems is a goal of global interest.

The unsubstituted S,N-bidentate ligands pyridine-2-thiolate (PyS) and pyrimidine-2-thiolate (PymS) have previously been used to synthesize dioxidomolybdenum(VI) complexes.[31,60−62] In addition to their favorable donor abilities and commercial availability, a remarkable property of such ligands is the tautomeric equilibrium between the thiolate and thione forms depending on the environment, making it a flexible donor appropriate for catalytic reactions (Figure 1).[63] Although the introduction of substituents is synthetically feasible, substituted systems are rather scarce and those known in the literature have been only poorly described.[62]

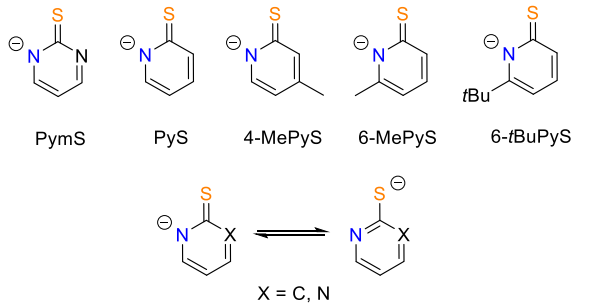

Figure 1. Pyrimidine- and pyridine-based S,N-bidentate ligands employed in this work listed in ascending order by electron donation and steric bulk. The tautomeric equilibrium between the thione and thiolate forms strongly depends on the environment.[63]

Herein, we utilized a series of S,N-bidentate ligands to probe the influence of electron donation and moderate steric bulk provided by the ligand framework on the OAT reaction rates: a weakly donating pyrimidine-2-thiolate (PymS), a more strongly donating pyridine-2-thiolate (PyS), a similarly strongly donating 4-methylpyridine-2-thiolate (4-MePyS) with a methyl group in a position with little steric influence, a more strongly donating 6-methylpyridine-2-thiolate (6-MePyS) with a methyl group close to the coordinating nitrogen atom, and eventually the best donor 6-*tert*-butylpyridine-2-thiolate (6-*t*BuPyS) bearing a sterically demanding substituent next to the coordinating nitrogen atom.

We report the preparation and characterization of four dioxidomolybdenum(VI) complexes employing four of the five aforementioned S,N-bidentate ligands. The catalytic activity of these complexes in OAT reactions involving the sulfoxides Me_2SO and Ph_2SO as well as the more challenging substrate NO_3^- as oxygen donors and both PPh_3 and PMe_3 as oxygen acceptors has been investigated, and intermediate species of the catalytic cycle have been isolated and characterized. Experimental results are also supported by DFT calculations. Eventually, the molecular structures of some unusual by-products are presented, providing a deeper insight into the versatility and reactivity of our molybdenum compounds.

■ RESULTS AND DISCUSSION

Synthesis of Dioxidomolybdenum(VI) Complexes. The molybdenum(VI) compounds $[MoO_2(PymS)_2]$ (**1**), $[MoO_2(PyS)_2]$ (**2**), $[MoO_2(4\text{-}MePyS)_2]$ (**3**), and $[MoO_2(6\text{-}MeSPy)_2]$ (**4**) are readily accessible by reaction of MoO_2Cl_2 or $MoO_2Cl_2(DMF)_2$ with 2.1 equiv of the sodium salt of the respective ligand in acetonitrile for no longer than 1 h (Scheme 1). Presumably due to too much steric hindrance directly next

Scheme 1. Synthesis of Dioxidomolybdenum(VI) complexes 1−4 Employing Four Different S,N-bidentate Ligands

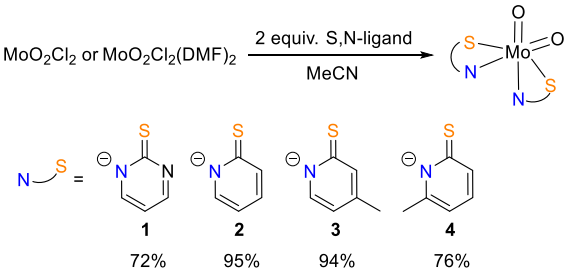

to the coordinating nitrogen atom, the preparation of a molybdenum complex employing 6-*t*BuPyS as a bidentate ligand has been unsuccessful.[64]

Similar to a literature procedure,[60] complex **1** was successfully isolated after the reaction of MoO_2Cl_2 with Na(PymS) by extraction with acetonitrile and subsequent precipitation by evaporation and addition of Et_2O. Due to its moderate solubility in acetonitrile, $[MoO_2(PymS)_2]$ was isolated as a dark yellow microcrystalline powder in only 72% yield. Interestingly, it shows good solubility in DMSO but only moderate solubility in THF and chlorinated hydrocarbons. Although it previously has been claimed that the literature-known complex **2** is not accessible in pure form by using $MoO_2Cl_2(DMF)_2$ as the metal precursor,[60] it was discovered that it is even more suitable than MoO_2Cl_2: with $MoO_2Cl_2(DMF)_2$ as the starting material, compound **2** could be isolated as ocher crystals in 95% yield, whereas with MoO_2Cl_2, the reaction mixture turned red-purple after 10 min of stirring, which is indicative of dimer formation. In addition, the presence of the protonated ligand after workup was revealed by ^{1}H NMR spectroscopy. With regard to ligand design, a methyl group in the *para* position of the pyridine ring does not have any obvious influence on the properties of the resulting dioxidomolybdenum(VI) compound: the reaction with 4-MePyS as the ligand proceeds similarly, the workup is equal, and complex **3** has the same appearance and is accessible in a yield identical with that of **2**. In contrast, a methyl group in an *ortho* position seems to have more impact: especially when the reaction mixture is stirred for longer than 1 h in acetonitrile, the reaction of $MoO_2Cl_2(DMF)_2$ with 2.1 equiv of Na(6-MePyS) is much more prone to formation of 2,2′-bis(6-methylpyridyl) disulfide, which was confirmed by comparing ^{1}H NMR data with the literature values.[65] Since an oxidation of sulfide is taking place, some other species must be reduced: this fairly interesting compound was revealed to be $[\{MoO(6\text{-}MePyS)(6\text{-}MePySH)\}_2(\mu\text{-}O)_2]$ (**5**) (Figure 2) by single-crystal X-ray diffraction analysis after crystallization from dichloromethane/heptane. In this molybdenum(V) dimer, the metal centers are coordinated not only by one oxido, two μ-oxido, and one monoanionic 6-MePyS in a bidentate fashion but also by the sulfur of a protonated 6-MePyS. Unfortunately, it has not been possible to selectively synthesize dimer **5**.

Nevertheless, the desired complex **4** was eventually isolated by evaporation of the solvent after 20 min, subsequent uptake

https://dx.doi.org/10.1021/acs.inorgchem.0c02412
Inorg. Chem. XXXX, XXX, XXX−XXX

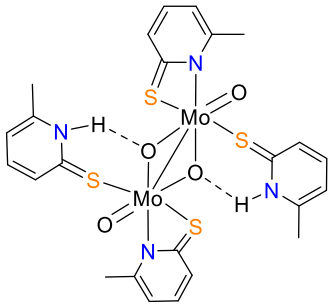

Figure 2. Dimeric molybdenum(V) compound [{MoO(6-MePyS)(6-MePySH)}$_2$(μ-O)$_2$] (**5**) isolated during attempts to synthesize [MoO$_2$(6-MePyS)$_2$] (**4**).

of the residue in toluene, filtration through Celite to remove NaCl, evaporation of the filtrate, and washing of the resulting precipitate with acetonitrile. At 76%, the yield of this reaction is not as good as with the other pyridine ligands. Complexes **3** and **4** exhibit good solubility and stability in chlorinated hydrocarbons, THF, toluene, and DMSO and poor solubility in acetonitrile, diethyl ether, and hydrocarbons. The IR spectra of complexes **1**−**4** show two strong bands indicative of ν(Mo═O) which are very similar in all compounds: for complex **1**, the ν(Mo═O) peaks appear at 933 and 897 cm^{-1}, for complex **2** at 926 and 896 cm^{-1}, for complex **3** at 922 and 894 cm^{-1}, and for complex **4** at 928 and 896 cm^{-1}. These data are in agreement with the literature values of neutral dioxidomolybdenum(VI) complexes.[31,45,60] Furthermore, ^{1}H and ^{13}C NMR spectra confirmed the identity and purity of complexes **1**−**4**. All complexes exclusively form one isomer in solution as well as in the solid state (*vide infra*).

The crystal structures of complexes **2**−**4** were determined by single-crystal X-ray diffraction analysis at 100 K. Complexes **2** and **3** were recrystallized from acetonitrile, whereas single crystals of **4** were obtained from dichloromethane/heptane at −37 °C. Molecular views of **2**−**4** are given in Figure 3, and selected bond lengths and angles of complexes **1**−**4** are compared in Table 1.[61] Full crystallographic details such as structure refinement as well as experimental details are provided within the Supporting Information.

In complexes **1**−**4**, the molybdenum center is coordinated by two S,N-bidentate ligands and two oxido ligands in a distorted-octahedral fashion. As already observed in the room-temperature structure determination of **2**, the complexes exhibit an *S,S-trans* configuration with the N atoms in positions *cis* to each other.[60] The determined Mo−O bond distances fall in the expected ranges for dioxidomolybdenum(VI) complexes.[66] The two Mo−N bonds in **4** are considerably longer than those in **3**, demonstrating the influence of the methyl group next to the nitrogen, whereas the Mo−S bond distances are almost identical. Interestingly, ∠S1−Mo1−S2 is greater by 5° in compound **4**.

Furthermore, the molecular structure of dimer **5** was determined by single-crystal X-ray diffraction analysis. A molecular view of compound **5** is given in Figure 4, and selected bond lengths and angles are shown in Table 2.

Complex **5** is arranged around a 2-fold rotation axis. To each Mo atom, an S,N-bidentate ligand is bound with its N atom *trans* to the terminal oxido ligand and with its S atom *trans* to a bridging oxido ligand. The O atoms as well as the N atoms are almost eclipsed (O1−Mo1−Mo1′−O1′ 6.42(5)°, N11−Mo1−Mo1′−N11′ −5.67(4)°). The octahedral environment of the Mo atom is completed by the S atom of a neutral 6-methylpyridine-2-thione *trans* to the other μ-oxido ligand (O2′−Mo1−S2 161.26(3)°). The orientation of this neutral ligand is presumably determined by a strong intramolecular hydrogen bond to a μ-oxido ligand (see Table 2). The least-squares planes through the ring atoms of the two ligands enclose an angle of 81.66(6)°. The Mo1−Mo1′ distance lies in the same range as in literature-known μ-oxido molybdenum(V) dimers bearing two parallel oxido ligands and a sulfur- and nitrogen-rich ligand environment.[67−72] On direct comparison to the Mo1−Mo1′ distance in the structurally most similar dimers [{MoO(PymS)(Py)}$_2$(μ-O)$_2$][67] and [{MoO(SPh)(mbipy)}$_2$(μ-O)$_2$][72] (2.577 and 2.584 Å), the metal−metal bond length of 2.60 Å in **5** is practically identical.

Reduction with PPh$_3$. In order to investigate their catalytic applicability, the behavior of complexes **1**−**4** toward stoichiometric reduction with PPh$_3$ and PMe$_3$ was investigated in the first place. The reactions of **1** and **2** with PPh$_3$ yielding

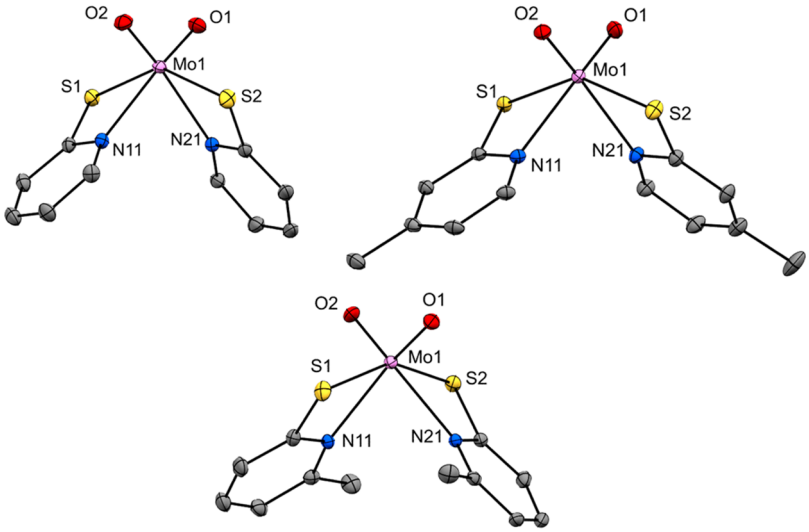

Figure 3. Molecular structures (50% probability thermal ellipsoids) of complexes **2** (top left), **3** (top right), and **4** (bottom) showing the atomic numbering scheme. H atoms are omitted for clarity.

https://dx.doi.org/10.1021/acs.inorgchem.0c02412
Inorg. Chem. XXXX, XXX, XXX−XXX

Table 1. Selected Bond Lengths (Å) and Angles (deg) for Complexes 1[61] and 2−4

	1	2	3	4
Mo1−O1	1.696(5)	1.7053(10)	1.7065(13)	1.7054(12)
Mo1−O2	1.693(5)	1.7116(9)	1.7111(14)	1.7118(12)
Mo1−N11	2.332(5)	2.3085(10)	2.3178(13)	2.3934(13)
Mo1−N21	2.317(5)	2.2938(10)	2.2954(14)	2.3478(12)
Mo1−S1	2.433(2)	2.4435(3)	2.4388(4)	2.4299(5)
Mo1−S2	2.456(2)	2.4538(4)	2.4538(4)	2.4383(5)
∠O1−Mo1−O2	107.3(3)	106.92(5)	106.79(7)	106.57(6)
∠O1−Mo1−N11	156.5(2)	156.45(4)	155.14(6)	153.80(6)
∠O2−Mo1−N21	153.5(2)	156.59(4)	155.87(6)	153.59(5)
∠N11−Mo1−N21	74.8(2)	77.06(4)	79.16(5)	80.10(4)
∠S1−Mo1−S2	146.01(6)	144.523(12)	147.378(15)	152.160(15)

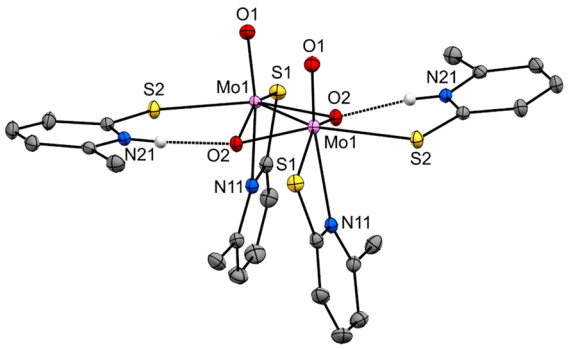

Figure 4. Molecular structure (50% probability thermal ellipsoids) of dimer **5**. With the exception of those involved in hydrogen bonding, H atoms are omitted for clarity.

Table 2. Selected Bond Lengths (Å) and Information on Hydrogen Bonds for Complex 5

Mo1−O1	1.6874(10)
Mo1−O2	1.9467(9)
Mo1−O2	1.9638(9)
Mo1−N11	2.3848(11)
Mo1−S1	2.5212(3)
Mo1−S2	2.5622(3)
Mo1−Mo1′	2.6017(2)
N21−H21	0.88
H21···O2	1.822(4)
N21···O2	2.6725(13)
∠N21−H21···O2	161.8(11)°

the molybdenum(V) dimers $[Mo_2O_3(PymS)_4]$ (**6**) and $[Mo_2O_3(PyS)_4]$ (**7**), respectively, have previously been described in the literature.[60] However, we were unable to reproduce the reported macroscopic behavior and spectroscopic data of the compounds. In our hands, the deep purple materials obtained after reactions of **1** and **2** as well as of **3** and **4** with 0.6 equiv of PPh_3 in acetonitrile were found to be poorly soluble in any solvent. The purple color[73,74] is nonetheless consistent with the formation of dimers of the type $[Mo_2O_3L_4]$ (L = PymS (**6**), PyS (**7**), 4-MePyS (**8**), 6-MePyS (**9**)), as shown in Scheme 2. This assumption is particularly supported by IR spectroscopy and also by elemental analysis and the molecular structure of **8** (*vide infra*).

The low solubility prevented the recording of meaningful ^{1}H NMR data. This is on the one hand in accordance[31,75] yet on the other hand in contrast to the literature with reported NMR data for $[Mo_2O_3(PyS)_4]$ (**7**) in acetone-d_6[60] as well as in

Scheme 2. Synthesis of Molybdenum(V) Dimers 6−9 by Reduction of Complexes 1−4 with 0.5 equiv of PPh_3

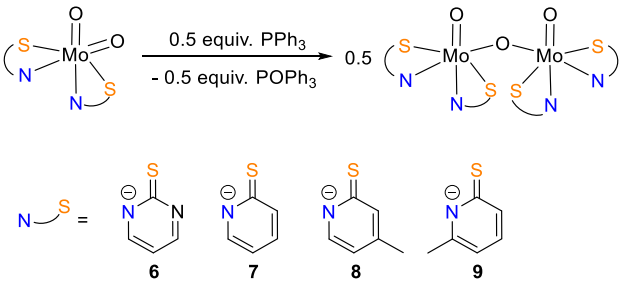

chloroform-d.[62] Interestingly, the latter gives data identical with our data for the dioxido compound $[MoO_2(PyS)_2]$ (**2**), which points toward residual **2** in the reported spectra presumably due to an incomplete reaction. Also IR data are practically identical with values obtained for **2** in this work. The IR spectra of products **6**−**9** show a sharp band characteristic of ν(Mo═O) in the region from 947−930 cm^{-1}, which is consistent with literature values of similar systems.[60,74,76] When the spectra are compared with those of the corresponding dioxido complexes, an additional band of weak intensity at ∼440 cm^{-1} is present in all complexes, which can be ascribed to δ(Mo−O−Mo).[77−79] The asymmetric Mo−O−Mo stretch, which is usually found at ∼750 cm^{-1}, cannot be assigned in **6** and **9** due to overlapping with ligand vibrations, while in dimers **7** and **8**, the bands at 775 and 785 cm^{-1}, respectively, can explicitly be ascribed to ν(Mo−O−Mo).[79] When **6**−**9** are suspended in DMSO-d_6, there are no NMR signals that could be assigned to the complexes. However, the dimers slowly react back to the respective dioxidomolybdenum(VI) complexes **1**−**4** in an OAT reaction, suggesting that molybdenum(V) dimers might be catalytically active, which is in accordance with previously reported results.[62] While the reaction is complete for **6** and **7**, a considerable amount does not react back to the respective molybdenum(VI) compound but remains undissolved as a black precipitate in case of **8** and **9** after approximately 1 week.

Single crystals of dimer **8** were obtained from a dichloromethane reaction solution at rt, and the molecular structure was determined by a single-crystal X-ray diffraction analysis. A molecular view is given in Figure 5. Selected bond lengths and angles along with full crystallographic details such as structure refinement as well as experimental details are provided within the Supporting Information.

https://dx.doi.org/10.1021/acs.inorgchem.0c02412
Inorg. Chem. XXXX, XXX, XXX−XXX

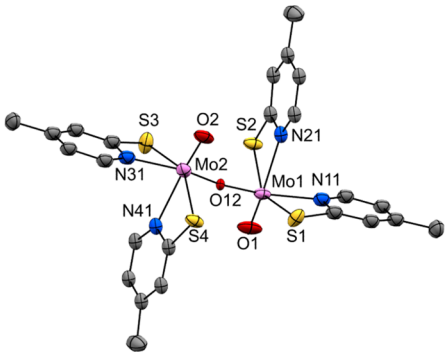

Figure 5. Molecular structure (50% probability thermal ellipsoids) of complex **8** showing the atomic numbering scheme. Hydrogen atoms are omitted for clarity.

Dimer **8** is almost centrosymmetric, with the oxido ligands in *trans* positions (Mo1−O1 1.676(6) Å, Mo2−O2 1.689(5) Å; O1−Mo1···Mo2−O2 178.9(3)°). The two distorted octahedra are linked by a μ-oxido ligand (O12−Mo1 1.855(4) Å, O12−Mo2 1.851(3) Å; Mo2−O12−Mo1 170.4(3)°). As observed for the unsubstituted[62,80] and the trimethylsilyl-substituted pyridine-2-thiolate complex,[74] the bidentate ligands with the N atoms *trans* to O12 (O12−Mo1−N11 154.0(2)°; O12−Mo2−N31 155.7(2)°) show distinctly shorter distances to the metal center (Mo−N 2.170(6)−2.189(6) Å, Mo−S 2.443(6)−2.451(6) Å vs Mo−N 2.309(8)−2.295(8) Å, Mo−S 2.501(2)−2.507(2) Å) in comparison to those *trans* to the terminal oxido ligands (O1−Mo1−N21 155.8(3)°, O2−Mo2−N41 156.8(3)°).

UV−Vis Spectroscopy. The kinetics of the stoichiometric oxygen atom transfer of one oxido ligand of complexes **1**−**4** to PPh_3 was investigated by UV−vis spectroscopy. The reactions were carried out in acetonitrile at 25 °C with an excess of PPh_3 (50, 100, and 150 equiv) to induce pseudo-first-order conditions. Screening the reactions with varying excess amounts of PPh_3 allowed the determination of the second-order rate constants (Table 3). UV−vis spectra with complexes **1**−**3** exhibit isosbestic points indicating clean OAT reactions and thus the formation of one distinct species (see Figure S34). The increase in absorbance at λ_{max} = 495 (**1**), 502 (**2**), and 504 nm (**3**), respectively, was followed (see Figure 6). By using the Eyring equation, $\Delta G^{\ddagger}$ values were determined from the rate constants k_2 at 25 °C (see Table 3).

Table 3. OAT Reaction Rates for Complexes 1−3

complex	k_2(M^{-1} s^{-1})	$\Delta G^{\ddagger}$ (kJ mol^{-1})
$[MoO_2(PymS)_2]$ (**1**)	0.50	75
$[MoO_2(PyS)_2]$ (**2**)	0.11	78
$[MoO_2(4\text{-}MePyS)_2]$ (**3**)	0.087	79

The reaction rate for $[MoO_2(PymS)_2]$ (**1**) was found to be 5 times faster in comparison to **2** and **3** (Table 3). However, with longer reaction time, a decrease in the absorbance at λ_{max} = 495 nm is observed, indicating that the reduced complex reacts further with an excess of PPh_3, possibly upon further reduction or ligand substitution. Such reactivity is not observed with a smaller excess of PPh_3 (<10 equiv) and is not at all observed with complexes **2** and **3**. In contrast, the reaction of $[MoO_2(6\text{-}MePyS)_2]$ (**4**) with excess PPh_3 does not lead to any conclusive results: after a solution of **4** is combined with PPh_3, the reaction solution changes immediately from light yellow to pink within a few seconds and then starts to get pale again, suggesting a very fast reaction and a further reaction. Therefore, no rate constant could be determined.

Reduction with PMe_3. Reduction of **1**−**4** with the electron-rich and sterically less demanding PMe_3 in comparison to PPh_3[81] led to the monomeric complexes $[MoOL_2(PMe_3)_2]$ (L = PymS (**10**), PyS (**11**), 4-MePyS (**12**)) and $[MoO(6\text{-}MePyS)_2(PMe_3)]$ (**13**), as displayed in Scheme 3. While the latter 16e$^-$ species with one coordinated PMe_3 is quite common,[82−85] the formation of the 18e$^-$ complexes with two coordinated PMe_3 donors was rather unexpected. To the best of our knowledge, this behavior of dioxidomolybdenum(VI) complexes toward PMe_3 is unique. It is mainly explained by the absence of relevant steric hindrance in the ligand framework.

Complexes **10**−**13** were prepared by addition of a diluted PMe_3 solution to a solution of $[MoO_2L_2]$ (**1**−**4**) in acetonitrile and/or dichloromethane. After workup, the oxidomolybdenum(IV) compounds were isolated as intensively colored powders in very good yield. Using exactly 2 equiv of PMe_3 to enforce the formation of the 16e$^-$ complex with only one coordinated PMe_3 led to mixtures of $[MoOL_2(PMe_3)_2]$ and dimeric species, which reveals complexes **10**−**12** to be the thermodynamically stable products of the reduction with PMe_3. In contrast, for the preparation of $[MoO(6\text{-}MePyS)_2(PMe_3)]$ (**13**) in good yield, we found 2.6 equiv of PMe_3 to be optimal, as smaller amounts led to incomplete reactions and greater amounts to side product formation. Compounds **10**−**13** are highly soluble in dichloro-

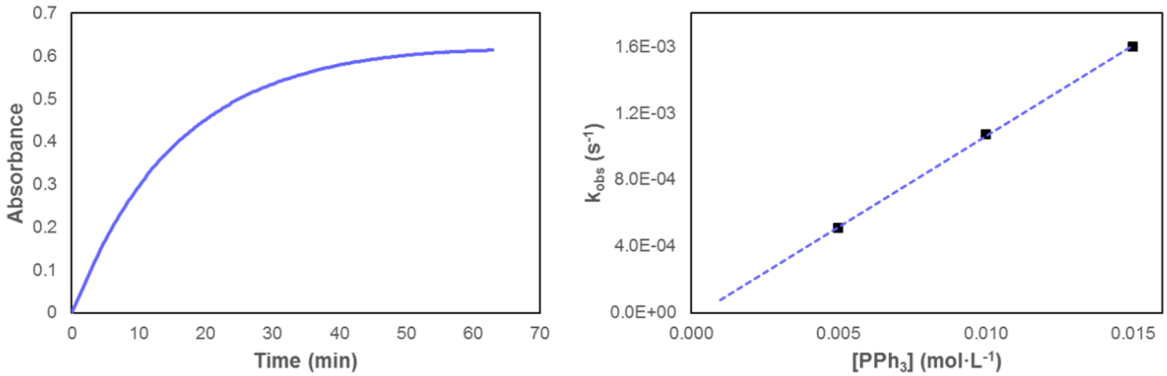

Figure 6. (left) Determination of k_{obs} at λ = 505 nm and [PPh_3] = 10 mmol L^{-1} for $[MoO_2(PyS)_2]$ (**2**). (right) Determination of k_2 for $[MoO_2(PyS)_2]$ (**2**).

https://dx.doi.org/10.1021/acs.inorgchem.0c02412
Inorg. Chem. XXXX, XXX, XXX−XXX

Scheme 3. Synthesis of Oxidomolybdenum(IV) Complexes 10−13 by Reduction of 1−4 with 2 and 3 equiv of PMe_3, Respectively

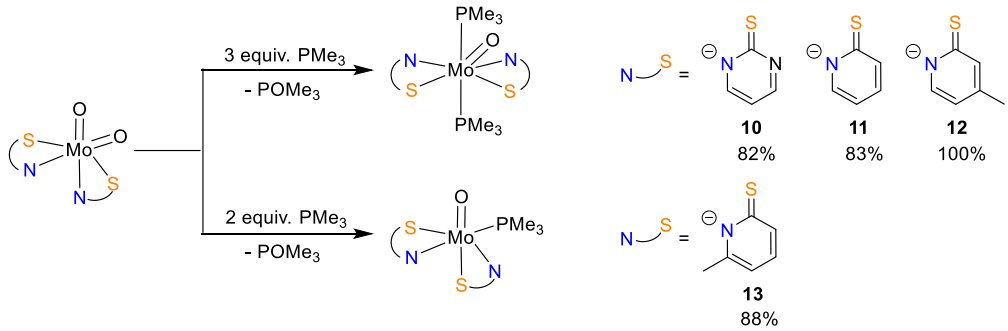

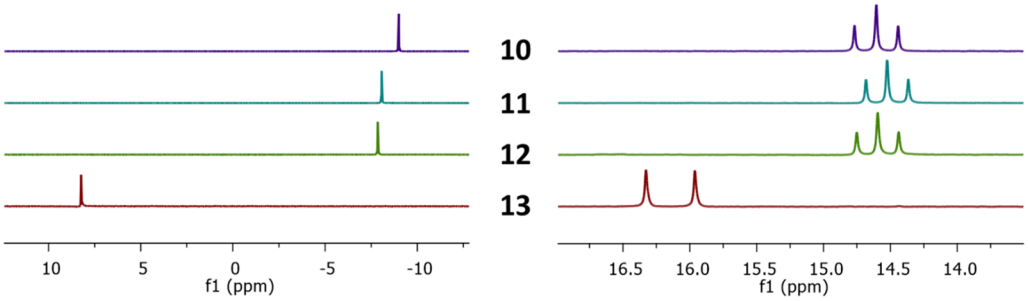

Figure 7. Resonances of coordinated PMe_3 in $^{31}P\{^1H\}$ (left) and ^{13}C (right) NMR spectra of complexes **10−13**.

methane, THF, and toluene and poorly soluble in diethyl ether and hydrocarbons. In contrast to **11** and **12**, complex **10** is also quite soluble in acetonitrile. Although they all exhibit high solubility in chloroform as well, **11** and **12** start to decompose within a few days and **13** even within 5 h by reacting with the solvent, whereas **10** is completely stable for 1 week. The IR spectra of compounds **10−13** show one strong band indicative of ν(Mo═O) at ∼940 cm^{-1}. These data are in accordance with literature values of rather rare oxidomolybdenum(IV) complexes with a coordinated trimethylphosphine.[29,82,86] In solution, compounds **10−13** exhibit only one isomer as determined by NMR spectroscopy. Despite the coordination of two PMe_3 groups, the $^{31}P\{^1H\}$ NMR spectrum of complexes **10−12** shows a sharp singlet (−9.00 ppm for **10**, −8.07 ppm for **11**, and −7.86 ppm for **12**), which is indicative of highly symmetric complexes in which the two PMe_3 groups are coordinated opposite to each other. The phosphorus of the coordinated PMe_3 in compound **13** resonates at 8.23 ppm. This drastic downfield shift in comparison to complexes **10−12** is explained by a different ligand in the *trans* position. In the ^1H NMR spectrum of complexes **10−12**, the protons of the two coordinated PMe_3 groups display a virtual triplet at δ ∼1.25 ppm integrating for 18 protons. In the ^{13}C NMR spectrum, the carbons of the coordinated PMe_3 also give a triplet. The appearance of these triplets is caused by virtual coupling: in a three-spin system (PP′H and PP′C), the observed nucleus appears to be coupled to both of the other nuclei even though it is only coupled to one of them.[87] This effect is promoted by the strong coupling of the two opposite phosphorus nuclei. For complex **13**, in contrast, a doublet is observed in the ^1H NMR as well as in the ^{13}C NMR spectrum since there is only one PMe_3 group coordinated. The parts of $^{31}P\{^1H\}$ and ^{13}C NMR spectra of complexes **10−13** that show the resonances of the coordinated PMe_3 are depicted in Figure 7.

When complexes **10−13** are dissolved in DMSO, the solutions change from deep orange-brown (**10**) or green (**11−13**) to deep purple (**10−12**) or deep red (**13**) within a few seconds. ^1H NMR spectroscopy demonstrates the formation of the respective dioxidomolybdenum(VI) complexes **1−4** along with $POMe_3$ and intensively colored intermediate Mo(IV) and/or Mo(V) species. After 5 h, compounds **10**, **11**, and **13** are fully converted to the respective dioxidomolybdenum(VI) complexes and $POMe_3$, resulting in a yellow solution. In case of $[MoO(4\text{-}MePyS)_2(PMe_3)_2]$ (**12**), a respectable amount does not react to the respective molybdenum(VI) compound **3** but remains undissolved as a dark green precipitate after a few days. The findings suggest that complexes **10−13** might be intermediates in a catalytic OAT reaction between DMSO and PMe_3.

As already mentioned above, $[MoO(6\text{-}MePyS)_2(PMe_3)]$ (**13**) is not stable in chloroform, but also $[MoO(4\text{-}MePyS)_2(PMe_3)_2]$ (**12**) shows some reactivity toward the solvent. On two occasions, we were able to isolate single crystals of side products which allowed the determination of their structures by an X-ray diffraction analysis. In the dimer $[\{MoO(4\text{-}MePyS)(\mu\text{-}4\text{-}MePyS)\}(\mu\text{-}O)\{Mo(4\text{-}MePyS)_2(PMe_3)\}]$ (**12a**; *vide infra*), which crystallized from chloroform during an NMR experiment after reaction of $[MoO_2(4\text{-}MePyS)_2]$ (**3**) with PMe_3, one molybdenum is formally in oxidation state +V while the other is in the +III state. It was probably formed due to a lack of PMe_3 in the reaction solution. Similarly, the dimeric complex $[\{MoO(6\text{-}MePyS)(PMe_3)\}_2(\mu\text{-}O)_2]$ (**13a**; *vide infra*) crystallized from dichloromethane during an NMR experiment after the reaction of $[MoO_2(6\text{-}MePyS)_2]$ (**4**) and PMe_3. It is a typical molybdenum(V) dimer with two bridging and two parallel terminal oxido ligands similar in structure to dimer **5** (*vide supra*). It is presumably formed under oxidation of two ligands

https://dx.doi.org/10.1021/acs.inorgchem.0c02412
Inorg. Chem. XXXX, XXX, XXX−XXX

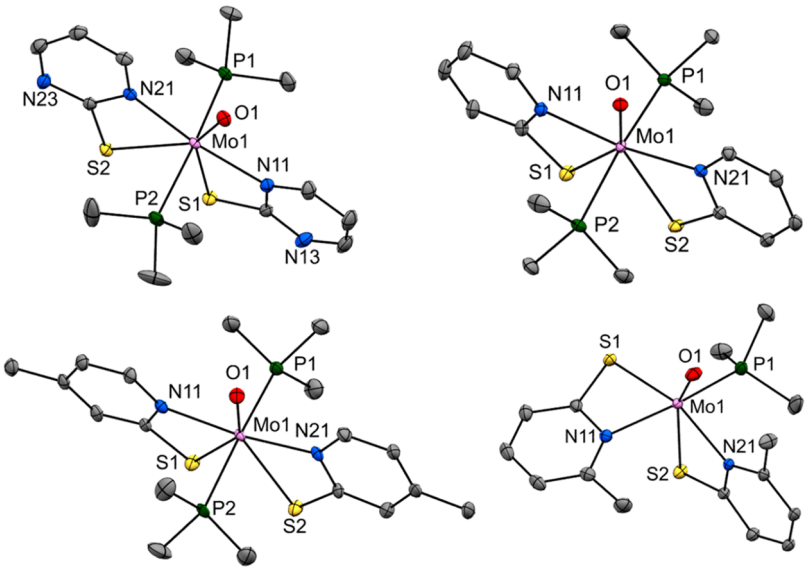

Figure 8. Molecular structures (50% probability thermal ellipsoids) of complexes **10** (top left), **11** (top right), **12** (bottom left), and **13** (bottom right) showing the atomic numbering scheme. Hydrogen atoms as well as solvent molecules are omitted for clarity.

Table 4. Selected Bond Lengths (Å) and Angles (deg) for Complexes 10−13

	10	11	12	13
Mo1−O1	1.7115(13)	1.7190(11)	1.719(3)	1.6832(10)
Mo1−N11	2.2084(17)	2.2228(13)	2.220(4)	2.2122(12)
Mo1−N21	2.2072(16)	2.2234(13)	2.220(4)	2.2131(11)
Mo1−P1	2.5023(5)	2.4910(4)	2.4976(14)	2.4611(4)
Mo1−P2	2.5080(6)	2.4994(4)	2.4933(14)	
Mo1−S1	2.6880(5)	2.6906(4)	2.6883(12)	2.4386(4)
Mo1−S2	2.7006(5)	2.6891(4)	2.6929(12)	2.6557(4)
∠N11−Mo1−N21	168.33(6)	165.83(5)	167.33(12)	103.09(4)
∠P1−Mo1−P2	169.654(19)	168.946(14)	171.40(4)	
∠O1−Mo1−N11	83.81(7)	82.89(5)	83.73(15)	104.71(5)
∠N11−Mo1−S1	61.11(5)	61.08(4)	61.23(11)	66.79(3)
∠S1−Mo1−S2	70.649(16)	72.219(12)	71.09(3)	94.555(12)
∠S2−Mo1−N21	60.98(5)	61.22(4)	61.06(11)	63.21(3)
∠N21−Mo1−O1	84.51(7)	82.94(5)	83.61(15)	94.38(5)
∠O1−Mo1−S1	144.28(5)	143.79(4)	144.54(12)	107.91(4)
∠O1−Mo1−S2	145.06(5)	143.99(4)	144.37(12)	157.52(4)
∠N11−Mo1−S2	130.63(5)	132.91(4)	131.49(11)	83.33(3)
∠N21−Mo1−S1	130.45(5)	133.06(3)	131.42(11)	157.10(3)
∠N11−Mo1−P1	91.67(5)	90.28(4)	90.59(11)	155.82(3)
∠O1−Mo1−P1	94.53(5)	94.79(4)	94.39(14)	96.56(4)

to the corresponding disulfide, which we observe quite regularly in decomposed complex solutions.

Single crystals of complexes **10−13** were obtained from dichloromethane/heptane at −37 °C. Molecular views of compounds **10−13** are given in Figure 8, and selected bond lengths and angles are shown in Table 4. Full crystallographic details such as structure refinement as well as experimental details are provided within the Supporting Information.

The pentagonal-bipyramidal surrounding of the molybdenum center in complexes **10−12** consists of two trimethylphosphine ligands as apexes and one oxido ligand and two S,N-bidentate ligands with rather large Mo−S distances in the equatorial plane. The Mo−ligand bond distances are almost identical in all three compounds, and the angles given in Table 4 are fairly similar as well. Until now, more than 10 crystal structures of mononuclear molybdenum complexes in which the metal center is coordinated in a pentagonal-bipyramidal fashion with two trimethylphosphine molecules in *trans* positions are known in the literature.[88−97] However, there are none with two bidentate ligands. The distorted-octahedral surrounding of the molybdenum center in complex **13** consists of one oxido ligand, one trimethylphosphine, and two bidentate pyridine-2-thiolate ligands. The Mo−S distance *trans* to the oxido ligand (Mo1−S2 2.6557(4) Å) is distinctly longer than the other (Mo1−S1 2.4386(4) Å), although it is in the range of the Mo−S distances found in complexes **10−12**. The Mo−P distances are very similar in **10−12** and are approximately 0.04 Å longer than that in **13**. At first glance, a seven-coordinate complex of the type $[MoO(6\text{-Me-PyS})_2(PMe_3)_2]$ with 6-MePyS as the ligand seems feasible.

https://dx.doi.org/10.1021/acs.inorgchem.0c02412
Inorg. Chem. XXXX, XXX, XXX−XXX

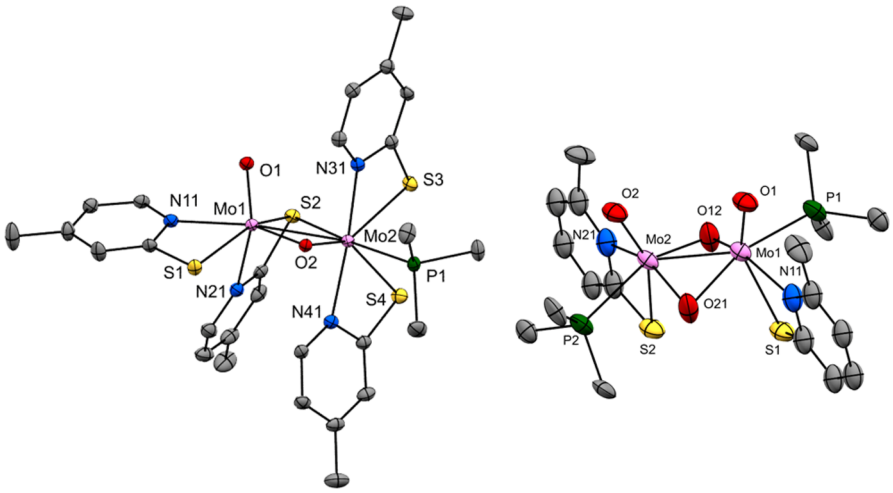

Figure 9. Molecular structures (50% probability thermal ellipsoids) of complexes **12a** (left) and **13a** (right) showing the atomic numbering scheme. Hydrogen atoms as well as solvent molecules are omitted for clarity.

However, considering a stepwise introduction of the phosphine, we assume that rather the attack of a second PMe_3 opposite to the already coordinated PMe_3 on the metal center is not favorable and that one PMe_3 is a sufficiently good donor to create a reasonably stable complex.

Molecular views of complexes **12a** and **13a** are given in Figure 9, and selected bond lengths and angles along with crystallographic details such as structure refinement as well as experimental details are provided within the Supporting Information.

The center of complex **12a** is built by an almost planar Mo_2OS ring with similar Mo−O (Mo1−O2 1.9554(19) Å, Mo2−O2 1.9286(19) Å) and Mo−S distances (Mo1−S2 2.4681(9) Å, Mo2−S2 2.4659(9) Å). The two Mo atoms in different oxidation states (*vide supra*) show quite different surroundings: the distorted-octahedral environment around Mo1 consists of two S atoms of two thiolate ligands in *trans* positions (Mo1−S1 2.4587(9) Å; S1−Mo1−S2 151.37(3)°) and two N atoms of the same thiolate ligands. The Mo−N bond opposite the terminal oxido ligand (Mo1−N21 2.370(2) Å, Mo1−O1 1.6995(18) Å; O1−Mo1−N21 148.25(9)°) is distinctly longer than that *trans* to the μ-oxido ligand O2 (Mo1−N11 2.269(2) Å; O2−Mo1−N11 152.94(8)°). The other Mo atom exhibits a pentagonal-bipyramidal surrounding similar to that observed in complex **12** consisting of the μ-thiolate atom S2 and the trimethylphosphine ligand as apexes (Mo2−P1 2.5046(10) Å; S2−Mo2−P1 172.05(3)°) and one μ-oxido ligand and two *N,N-trans* 4-MePyS ligands with rather large Mo−S distances (Mo2−S3 2.5934(9) Å, Mo2−S4 2.6002(8) Å; S3−Mo2−S4 72.16(3)°) in the equatorial plane. In dimer **13a**, the Mo−O bond lengths in the folded central Mo_2O_2 ring are in the range 1.971(5)−2.056(5) Å. A 6-MePyS ligand is bound to each Mo atom with its N atom *trans* to a μ-oxido ligand (Mo1−N11 2.228(7) Å, O12−Mo1−N11 149.4(3)°; Mo2−N21 2.213(7) Å, O21−Mo2−N21 148.7(3)°) and with its S atom in a rather long distance *trans* to the terminal oxido ligand (Mo1−O1 1.737(13) Å, Mo1−S1 2.639(5) Å, O1−Mo1−S1 148.7(5)°; Mo2−O2 1.736(13) Å, Mo2−S2 2.665(5) Å, O2−Mo2−S2 149.6(4)°). The coordination sphere of the Mo atoms is completed by trimethylphosphine ligands *trans* to the other μ-oxido ligand (Mo1−P1 2.516(4) Å, O21−Mo1−P1 154.8(4)°; Mo2−P2 2.515(4) Å, O12−Mo2−P2 152.1(4)°). The terminal oxido ligands are almost eclipsed (O1−Mo1−Mo2−O2 1.0(10)°), as seen before in dimer **5** (*vide supra*).

Catalytic OAT with DMSO. The catalytic OAT reactivity of complexes **1**−**4** was probed with DMSO as an oxygen donor and both PPh_3 and PMe_3 as oxygen acceptors. The respective phosphine was used as the limiting factor. The reactions were performed at 20−22 °C in 0.5 mL of dry, deoxygenated DMSO-d_6 in J. Young NMR tubes to guarantee a water- and dioxygen-free atmosphere. The catalytic conversion of PPh_3 to $POPh_3$ and the oxidation of PMe_3 to $POMe_3$ was followed by ^{1}H NMR spectroscopy. The respective phosphine oxide has been detected as a single product, which means that the reaction is completely selective. The results of the catalytic OAT reactions are shown in Table 5.

With PPh_3 as an oxygen acceptor, the reaction proceeds generally much more quickly than with PMe_3. This significant difference is ascribed to the capability of PMe_3 to coordinate to the molybdenum center to form a stable complex (*vide supra*). On consideration of the OAT reaction between DMSO and

Table 5. Results of Catalytic OAT Reactions between DMSO and PPh_3 or PMe_3[a]

cat.	cat. loading (mol %)	conversion (%)	time (h)
	PPh_3		
1	1	100	2.5
1	0.5	100	5
2	5	100	10
2	1	100	48
3	5	100	17
3	1	100	>48
4	1	100	2.5
4	0.5	100	5.5
	PMe_3		
4	5	100	0.5
4	1	100	7

[a]Conditions: DMSO-d_6 (0.5 mL), PPh_3 (114 μmol) or PMe_3 (233 μmol), and catalyst (0.5−5 mol % with regard to PPh_3 or PMe_3). The full conversion of PPh_3 to $POPh_3$ and PMe_3 to $POMe_3$, respectively, was determined by ^{1}H NMR spectroscopy. All experiments were performed at least three times. In blank experiments without a metal complex, no conversion of PPh_3 to $POPh_3$ was observed.

https://dx.doi.org/10.1021/acs.inorgchem.0c02412
Inorg. Chem. XXXX, XXX, XXX−XXX

PPh_3, the catalytic cycle of which is shown in Figure 10, the reactivity difference among complexes **1**−**4** is remarkable, with

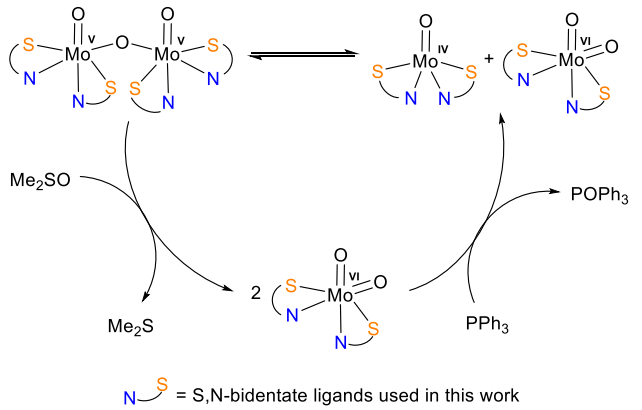

Figure 10. Proposed catalytic cycle for the OAT reaction between DMSO and PPh_3.[98]

1 and **4** exhibiting significantly higher activities in comparison to **2** and **3** (see Table 5). This finding is in accordance with the results of the kinetic experiments performed for **1**−**3**, suggesting that oxygen abstraction by the phosphine might be the rate-determining step of the reaction. The low performance of catalyst **2** is consistent with literature data,[31,60] and the similar behavior of complexes **2** and **3** reveals that the methyl group in a *para* position to nitrogen has only a slight influence on the reactivity. In contrast, complex **4** with the methyl group in an *ortho* position is a much more active catalyst, suggesting that steric hindrance next to a coordinating atom has a significant effect. From this point of view, it might be surprising that complexes **1** and **4** are equally active and even more so as the electronic properties of their ligand framework seem to be entirely different. However, on a closer look at the molybdenum−nitrogen bond lengths, it seems that 6-MePyS is not as tightly coordinated to the molybdenum center as 4-MePyS (see Table 1), making it a weaker electron donor than initially assumed. This theory is assured by the fact that 6-*t*BuPyS is not even capable of binding to the metal center with its sterically hindered nitrogen atom. With the methyl group in this special position, the electronic properties of 6-MePyS presumably resemble the character of PymS, which is thought to be a rather weak donor. Possibly, also the solubilities of the intermediately formed dimers **6**−**9**, respectively, influence the activity.

For the OAT reaction between DMSO and PMe_3, **4** is the only significantly active catalyst among the investigated complexes **1**−**4**. With a catalyst loading of 5 mol %, PMe_3 is fully converted to $POMe_3$ in 30 min when complex **4** is used, while with catalyst **2**, the reaction takes 8.5 h and with **1** and **3** several days. Similarly, with a catalyst loading of 1 mol %, PMe_3 is fully converted to $POMe_3$ in 7 h by applying catalyst **4** and with compounds **1**−**3** the conversion takes more than 2 weeks. This extremely low reaction rate of the latter results from the stability of the intermediately formed $18e^-$ complexes **10**−**12**, which are favorably formed when enough PMe_3 is present. Thus, dissociation of two coordinated PMe_3 groups seems to be the rate-determining step in the catalytic cycle shown in Figure 11. This step is entirely missing in the OAT reaction between PPh_3 and DMSO, since PPh_3 is not capable of coordination. With catalyst **4**, the intermediately formed

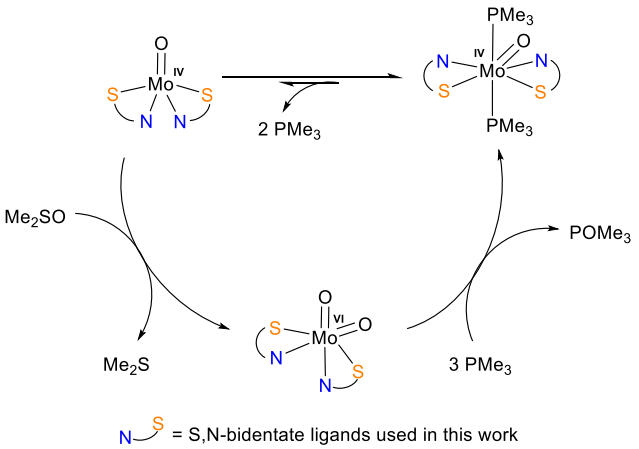

Figure 11. Proposed catalytic cycle for the OAT reaction between Me_2SO and PMe_3 catalyzed by complexes **1**−**3**.

compound **13** is only six-coordinate and therefore not as stable as compounds **10**−**12**, and only one PMe_3 has to decoordinate to enable further reaction. Due to its willingness to coordinate to a metal center, PMe_3 is not a recommended oxygen acceptor.

Catalytic OAT with Ph_2SO. Since PPh_3 turned out to be a suitable oxygen acceptor for catalytic reactions involving complexes **1**−**4**, two more substrates have been tested. A similar reactivity could be achieved with diphenyl sulfoxide as an oxygen donor, demonstrating the applicability of these complexes for a variety of sulfoxides. With dichloromethane-d_2 as solvent, the reactions were again performed under exclusion of dioxygen using an excess of Ph_2SO with regard to PPh_3. The results are shown in Table 6.

Table 6. Results of Catalytic OAT Reactions between Ph_2SO and PPh_3[a]

cat.	cat. loading (mol %)	conversion (%)	time (h)
1	10	100	7
1	1	85	24
2	10	100	26
3	10	100	39
4	10	100	2.5
4	1	100	16

[a]Conditions: CD_2Cl_2 (0.6 mL), PPh_3 (25 μmol), Ph_2SO (250 μmol), and catalyst (1−10 mol % with regard to PPh_3). The conversion of PPh_3 to $POPh_3$ was determined by ^{31}P NMR spectroscopy. All experiments were performed at least three times. In blank experiments without a metal complex, no conversion of PPh_3 to $POPh_3$ was observed.

Due to only a 10-fold excess of the sulfoxide, the OAT reactions with Ph_2SO take much longer than with DMSO, which was simultaneously used as a solvent. Under the conditions applied here, complex **4** is a better catalyst than **1**. Complexes **2** and **3** do not really qualify as active catalysts, since with a catalyst loading of 10 mol % they both need more than 24 h for full conversion of PPh_3 to $POPh_3$. Full conversion of PPh_3 to $POPh_3$ is also achieved with 1 equiv of Ph_2SO and 1 or 10 mol % catalyst loading, but the reactions are considerably slower.

Catalytic OAT with Nitrate. After showing that the deoxygenation of sulfoxides using complexes **1**−**4** and PPh_3 as an oxygen acceptor is generally possible, we wanted to proceed

https://dx.doi.org/10.1021/acs.inorgchem.0c02412
Inorg. Chem. XXXX, XXX, XXX−XXX

with the much more challenging and globally interesting substrate NO_3^-.[58,59] Since molybdenum complexes capable of (catalytic) nitrate reduction are rather scarce, the activity of complexes **1**−**4** toward tetrabutylammonium nitrate was explored. The reactions were carried out in dry dichloromethane-d_2 under exclusion of dioxygen with a catalyst loading of 10 mol % with regard to both nitrate and PPh_3, assuming that nitrate is fully reduced to N_2O via nitrite and NO using 2.5 equiv of PPh_3.[56,99] The results are shown in Table 7. Acetonitrile was also tested as a solvent, but solubility issues prevented the collection of meaningful data.

Table 7. Results of Catalytic OAT Reactions between $[Bu_4N][NO_3]$ and PPh_3

cat.	cat. loading (mol %)	conversion (%)	time (h)
1	10	22	3
2	10	12	4
3	10	12	5.5
4	10	15	2

[a]Conditions: CD_2Cl_2 (0.6 mL), PPh_3 (62.5 μmol), $[Bu_4N][NO_3]$ (25 μmol), and catalyst (2.5 μmol). The conversion of PPh_3 to $POPh_3$ was determined by ^{1}H NMR spectroscopy. All experiments were performed three times. In blank experiments without a metal complex, no conversion of PPh_3 to $POPh_3$ was observed within 24 h.

As already observed for Me_2SO and Ph_2SO, complexes **1** and **4** are more efficient catalysts than **2** and **3**, confirming the tendency toward more electron deficient ligand systems. For full conversion of the dioxido complexes **1**−**4** to their reduced molybdenum(IV) counterparts, 4% conversion of PPh_3 to $POPh_3$ would be expected, meaning that the rest of the total yields of 12−22% of $POPh_3$ given in Table 7 comes from nitrate, which is reduced to nitrite. However, depending on the catalyst, the reaction largely stops after 2−6 h and further oxidation of PPh_3 happens very slowly. After the catalyst solution is added to a solution of nitrate and PPh_3, the solution changes immediately to deep purple (**1** and **4**) or via red to deep purple (**2** and **3**), indicating an OAT from the dioxido complexes to PPh_3. During the reaction with Me_2SO or Ph_2SO as oxygen donors, the color stays the same until the end of the catalysis, while with nitrate, the solution changes to very light red (**1**), light yellow (**2** and **3**), or light orange-red (**4**) long before full conversion of PPh_3 to $POPh_3$ is reached, which indicates the formation of one or more species that are no longer catalytically active. In reaction solutions containing catalyst **1**, single crystals are formed after a few hours in both dichloromethane and acetonitrile. X-ray diffraction analysis of these crystals indeed revealed the formation of the highly interesting nitrosyl complex $[Mo(NO)(PymS)_3]$ (**14**), which is depicted in Figure 12. The linear bonding of the nitrosyl ligand in **14** suggests that NO donates one electron to the metal, making it a molybdenum(II) center coordinated by three PymS ligands and NO^+. The crystals were additionally characterized by EI-MS with $[Mo(NO)(PymS)_3]^+$ (m/z 461.0) and $[Mo(PymS)_3]^+$ (m/z 431.0) and by IR spectroscopy showing a strong band at 1665 cm^{-1}, which is characteristic of ν(N═O) in molybdenum complexes containing a NO^+ ligand. Nitrosyl molybdenum(II) complexes containing a Tp^{An} ligand show a ν(N═O) band at 1642−1676 cm^{-1}, and molybdenum(0) complexes with a coordinated NO^+ exhibit similar data.[100,101] Due to solubility issues with both acetonitrile and dichloromethane, no NMR data

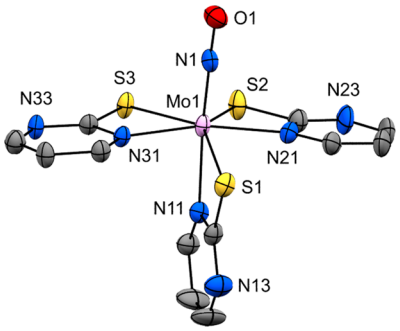

Figure 12. Molecular structure (50% probability thermal ellipsoids) of complex **14** showing the atomic numbering scheme. Hydrogen atoms as well as solvent molecules are omitted for clarity.

could be obtained. Interestingly, the pyridine-2-thiolate analogue of **14** has already been described solely in a crystal structure report.[102] In addition to this molybdenum(II) complex with three PymS ligands, a catalytically inactive, oxidized molybdenum species employing only one PymS must be formed, which we were unable to identify. Although no crystals could be obtained from reaction solutions containing catalysts **2**−**4**, there is presumably a similar situation going on. Nonetheless, the formation of the nitrosyl complex **14** simultaneously confirms the capability of **1** to reduce nitrate to nitrite and perhaps even further to NO and the reactivity toward NO, which inhibits the full conversion of nitrate. Nitrite and especially NO are capable of oxidizing PPh_3 to $POPh_3$ even without the presence of a catalyst;[99] hence, it is also possible that species generated from this reaction readily react with the molybdenum catalyst, thus inhibit the reduction of nitrate to nitrite. The one-electron reduction of nitrite to NO has also been a problem in an earlier report with the formation of a dinitrosyl molybdenum complex.[56]

Theoretical Calculations. The reversible dimer dissociation shown in Scheme 4 was evaluated by DFT calculations to elucidate its relevance in the catalytic cycle of OAT reactions.

Scheme 4. Reversible Dissociation of the μ-Oxido Molybdenum(V) Dimer to the Respective Monomeric Mo(IV) and Mo(VI) Complexes

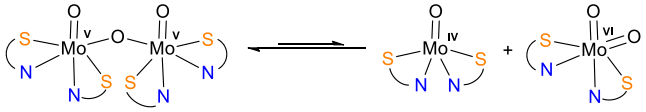

The free energies ΔG_{diss} of the dissociation equilibrium in the gas phase were determined by DFT calculations to assess the influence of the ligands investigated herein (PymS, PyS, 4-MePyS, 6-MePyS) on dimerization. The obtained values are summarized in Table 8.

Table 8. Dissociation Energies ΔG_{diss} Calculated for Dimers 6−9

dimer	ΔG_{diss} (kJ mol^{-1})
$[Mo_2O_3(PymS)_4]$ (**6**)	81.2
$[Mo_2O_3(PyS)_4]$ (**7**)	84.1
$[Mo_2O_3(4\text{-}MePyS)_4]$ (**8**)	66.5
$[Mo_2O_3(6\text{-}MePyS)_4]$ (**9**)	58.1

https://dx.doi.org/10.1021/acs.inorgchem.0c02412
Inorg. Chem. XXXX, XXX, XXX−XXX

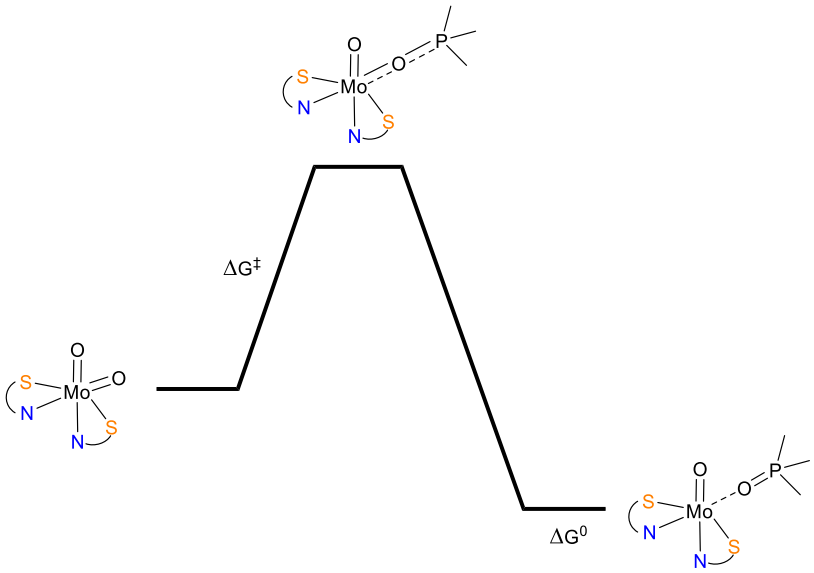

Figure 13. Reaction coordinate diagram of the first step of the OAT reaction in the investigated systems.

The computed values indicate that dimer formation is highly favored for all compounds. Due to the calculated dissociation energy difference of 23 kJ mol^{-1} between dimers **6** and **9**, these data cannot explain the similar catalytic activities of complexes **1** and **4**; thus, dimerization does not seem to play a rate-determining role in catalytic OAT with our complexes.

Therefore, the first step in the catalytic cycle, namely the abstraction of one oxygen atom by a phosphine, was computationally investigated for all complexes **1**−**4**. UV−vis spectroscopy allowed for the determination of experimental $\Delta G^{\ddagger}$ values from the rate constants by using the Eyring equation for **1**−**3** (see Table 3), but no data have been obtained for complex **4**. Thus, a complete comparison of the activation energy values for the oxygen abstraction involving complexes **1**−**4** is lacking. The initial step along the reaction coordinate for OAT to PMe_3, which is used for the calculations instead of the much larger PPh_3, involves nucleophilic attack of the phosphorus atom on one of the symmetry-equivalent oxido ligands. As the system approaches the transition state, the affected Mo═O bond lengthens with a concomitant decrease in the O−P distance, which is consistent with Mo═O bond weakening and nascent O−P bond formation. The O−P bond length at the transition state in complexes **1** and **4** (2.03 Å) is slightly longer than in complexes **2** and **3** (2.01 Å), while the Mo═O distances are practically identical. The corresponding reaction coordinate diagram is depicted in Figure 13. Since the detection of a coordinated OPR_3 has so far not been reported for pyrimidine- or pyridine-2-thiolate systems, it is assumed that these species are fairly short lived.[43,44,103]

The computed Gibbs free energy of activation, $\Delta G^{\ddagger}$, for the reaction between $[MoO_2(6\text{-MePyS})_2]$ (**4**) and PMe_3 was found to be 82.1 kJ mol^{-1} and therefore 3.9 kJ mol^{-1} lower than that for the reaction with $[MoO_2(PymS)_2]$ (**1**) (Table 9), which would imply that **4** is a better catalyst than **1**. Under the conditions chosen for the OAT from Ph_2SO to PPh_3, the theoretical results are perfectly reflected by the activity of the complexes. Under the applied conditions for the reduction of DMSO, they are equally active, which is mainly due to a huge excess of DMSO. The calculated $\Delta G^{\ddagger}$ values for $[MoO_2(PyS)_2]$ (**2**) and $[MoO_2(4\text{-MePyS})_2]$ (**3**) are slightly larger than for **1** and **4**, indicating a slower OAT, which is in good agreement with experimental results. When the computed values are compared with the experimental $\Delta G^{\ddagger}$ values for **1**−**3**, it is noticeable that they are of a very similar magnitude, though the computed barriers seem to be too high by 11−14 kJ/mol. The difference might arise from the fact that experimental barriers were obtained using PPh_3, while theoretical data are based on the reaction with PMe_3, which might have a slightly higher barrier. Nonetheless, the trend upon changing the ligand reflected in both experimental and theoretical studies suggests that this step is genuinely the rate-determining step of the catalytic reaction.

Table 9. Calculated Energies of the First Step of the OAT Reaction for Complexes 1−4

cat.	$\Delta G^{\ddagger}$ (kJ mol^{-1})	ΔG° (kJ mol^{-1})
$[MoO_2(PymS)_2]$ (**1**)	86.0	−71.3
$[MoO_2(PyS)_2]$ (**2**)	88.9	−64.0
$[MoO_2(4\text{-MePyS})_2]$ (**3**)	91.6	−58.3
$[MoO_2(6\text{-MePyS})_2]$ (**4**)	82.1	−66.9

For all complexes **1**−**4**, the O−P bond formation is exergonic, as showcased by negative ΔG° values (Table 9). It is most exergonic for **1** followed by **4**, **2**, and **3**, which is also somewhat in accordance with the experimental results. All values are comparable to recently published data on scorpionate complexes.[51]

■ CONCLUSIONS

Herein, the synthesis of four dioxidomolybdenum(VI) complexes of the general structure $[MoO_2L_2]$ (**1**−**4**) with S,N-bidentate ligands is reported. They were investigated as oxygen donors to the common oxygen acceptors PPh_3 and PMe_3, respectively. Since PPh_3 is not capable of coordinating to the metal center in our complexes, the formation of molybdenum(V) dimers **6**−**9** along with $POPh_3$ was observed. In contrast, the reaction of PMe_3 with **1**−**4** yielded complexes **10**−**13** with the molybdenum center in the oxidation state +IV. While $[MoOL_2(PMe_3)_2]$ (**10**−**12**) contain two molecules of PMe_3, complex **13** with the sterically more demanding 6-MePyS ligand comprises only one phosphine coordinated to the metal center, which has a significant effect on the reactivity.

https://dx.doi.org/10.1021/acs.inorgchem.0c02412
Inorg. Chem. XXXX, XXX, XXX−XXX

The results of the OAT between PPh_3 and Me_2SO, Ph_2SO, and nitrate catalyzed by complexes **1**−**4** suggest that rather weakly donating ligands have beneficial effects on the reaction rates. Theoretical calculations confirmed that in the catalytic OAT reaction between a phosphine and a sulfoxide, the rate-determining step is the abstraction of an oxygen atom of complexes **1**−**4** by PPh_3 or PMe_3. This step is facilitated by using a rather electron deficient ligand system, as demonstrated by a fast OAT with complexes **1** and **4**. The pyrimidine-based ligand PymS is less electron donating in comparison to the others, while 6-MePyS renders the metal less electron rich, since longer metal−nitrogen bond lengths are found in **4** due to steric hindrance provided by the methyl group in an *ortho* position. Steric effects are also crucial when it comes to the OAT reaction between PMe_3 and DMSO, since the coordination of one or even two PMe_3 groups leads to stabilized molybdenum(IV) complexes. Especially $18e^-$ complexes with the molybdenum center coordinated by two PMe_3 molecules are reluctant to undergo further reaction. In summary, the reactivity of the dioxidomolybdenum(VI) unit in pyrimidine- and pyridine-2-thiolate complexes can be fine-tuned by only small changes in the ligand design. As exemplified in this work, the positioning of a methyl group initiates remarkable reactivity differences. Therefore, the influence of various substituents in different positions ought to be more intensively investigated in the future.[39] Furthermore, our results show that complexes **1**−**4** are capable of catalyzing the most challenging step of nitrate reduction: namely that from nitrate to nitrite. In the catalytic reduction of nitrate with PPh_3, however, there are definitely other challenges to face in the future.

■ EXPERIMENTAL SECTION

General Considerations. All synthetic manipulations were performed under a nitrogen atmosphere using standard Schlenk and glovebox techniques. Solvents were purified via a Pure Solv Solvent Purification System. Chemicals were purchased from commercial sources and were used as received or dried under vacuum. The metal precursor MoO_2Cl_2 was purchased, whereas $MoO_2Cl_2(DMF)_2$ was readily synthesized according to a published procedure.[104] All glassware and Celite were dried at 100 °C prior to use. NMR spectra were recorded on a Bruker Avance III 300 MHz spectrometer at 22 °C. Chemical shifts δ are given in ppm. ^{1}H NMR spectra are referenced to residual protons in the solvent and ^{13}C NMR spectra to the deuterated solvent peak. The multiplicity of peaks is denoted as singlet (s), doublet (d), triplet (t), doublet of doublets of doublets (ddd), or multiplet (m). NMR solvents were stored over molecular sieves. Solid-state IR spectra were measured on a Bruker ALPHA ATR-FT-IR spectrometer at a resolution of 2 cm^{-1}. The relative intensity of signals is declared as strong (s), medium (m), weak (w), and very weak (vw). Elemental analyses (C, H, N, S) were performed at the Department of Inorganic Chemistry at the University of Technology in Graz using a Heraeus Vario Elementar automatic analyzer. Values for elemental analyses are given as percentages.

Ligand Synthesis. The ligand salts Na(PyS) and Na(PymS) were prepared by deprotonation of commercially available pyridine-2-thiol and pyrimidine-2-thiol, respectively, with pure NaH in THF. The ligands 4- and 6-methylpyridine-2-thiol were synthesized from 4- and 6-methylpyridin-2-amine, respectively, according to literature procedures.[65,105] The ligand 6-*tert*-butylpyridine-2-thiol was synthesized by starting from 3,3-dimethyl-2-butanone and ethyl formate following published procedures.[105,106] All three substituted thiones were then deprotonated by the same method as that for the unsubstituted analogue.

Complex Synthesis. In crystalline or microcrystalline form, all complexes are stable under ambient conditions for at least a few days but ought to be stored and handled under a nitrogen atmosphere for a longer period of time. Syntheses and ^{1}H NMR and IR data of complexes **1**, **2**, **6**, and **7** have been reported previously,[60−62,107] but modified syntheses and full spectroscopic data are provided herein.

*[MoO$_2$(PymS)$_2$] (**1**).* A mixture of MoO_2Cl_2 (597 mg, 3.00 mmol) and Na(PymS) (805 mg, 6.00 mmol) in 50 mL of MeCN was stirred for 2 h. The supernatant solution was removed, and the remaining solid was extracted with 200 mL of MeCN. After reduction of the volume to approximately 10 mL and subsequent addition of 30 mL of Et_2O, the resulting precipitate was isolated by filtration, subsequently washed with 8 mL of Et_2O, and dried *in vacuo* to give [$MoO_2(PymS)_2$] (1.01 g, 72%) as a dark yellow microcrystalline powder. ^{1}H NMR (DMSO-d_6, 300 MHz): δ 8.70 (d, J = 4.9 Hz, 4H, pymH-*o*), 7.36 (t, J = 4.9 Hz, 2H, pymH-*m*) ppm. ^{13}C NMR (DMSO-d_6, 75 MHz): δ 167.86 (s, 2C, C_q), 158.56 (s, 4C, pymC-*o*), 119.14 (s, 2C, pymC-*m*) ppm. IR (cm^{-1}): 1547 (s), 1427 (m), 1375 (s), 1262 (m), 1254 (m), 1177 (s), 933 (m, Mo═O), 897 (s, Mo═O), 821 (m), 800 (m), 762 (m), 748 (s), 653 (s), 474 (m). EI-MS (70 eV) m/z: M^+ 352.0.

*[MoO$_2$(PyS)$_2$] (**2**).* A solution of Na(PyS) (799 mg, 6.00 mmol) in 20 mL of MeCN was added dropwise to a stirred solution of $MoO_2Cl_2(DMF)_2$ (1.04 g, 3.00 mmol) in 10 mL of MeCN. The resulting yellow mixture was stirred for 45 min, whereupon the solvent was removed *in vacuo*. The ocher solid was suspended in 40 mL of CH_2Cl_2, and the resulting mixture was filtered through Celite. Thereafter, 20 mL of MeCN was added in order to crystallize the desired product by slow evaporation. After filtration and drying *in vacuo*, [$MoO_2(PyS)_2$] (988 mg, 95%) was isolated as ocher crystals suitable for X-ray diffraction analysis. ^{1}H NMR (CD_2Cl_2, 300 MHz): δ 8.47 (ddd, J = 5.4, 1.7, 0.9 Hz, 2H, pyH-*o*), 7.64 (ddd, 2H, pyH-*p*), 7.21 (ddd, J = 8.1, 1.0 Hz, 2H, pyH-*m*), 6.99 (ddd, J = 7.5, 5.4, 1.1 Hz, 2H, pyH-*m*) ppm. ^{13}C NMR (CD_2Cl_2, 75 MHz): δ 167.01 (s, 2C, C_q), 145.63 (s, 2C, pyC-*o*), 140.74 (s, 2C, pyC-*p*), 126.22 (s, 2C, pyC-*m*), 120.39 (s, 2C, pyC-*m*) ppm. IR (cm^{-1}): 1580 (s), 1556 (m), 1444 (m), 1422 (s), 1266 (m), 1134 (s), 926 (s, Mo═O), 894 (s, Mo═O), 751 (s), 726 (s), 644 (m), 480 (m), 455 (m). EI-MS (70 eV) m/z: M^+ 350.0. Anal. Calcd for $C_{10}H_8N_2O_2S_2Mo$: C, 34.49; H, 2.32; N, 8.04; S, 18.41. Found: C, 34.43; H, 2.34; N, 8.08; S, 18.12.

*[MoO$_2$(4-MePyS)$_2$] (**3**).* Na(4-MePyS) (927 mg, 6.30 mmol) was added portionwise to a stirred solution of $MoO_2Cl_2(DMF)_2$ (1.04 g, 3.00 mmol) in 30 mL of MeCN. The resulting intense yellow mixture was stirred for 45 min, whereupon the solvent was removed *in vacuo*. The yellow solid was then suspended in 40 mL of CH_2Cl_2, and the resulting mixture was filtered through Celite. Thereafter, 20 mL of MeCN was added to crystallize the desired product by slow evaporation. After filtration and drying *in vacuo*, [MoO_2(4-MePyS)$_2$] (1.06 g, 94%) was isolated as an ocher microcrystalline powder. Single crystals suitable for X-ray diffraction analysis were obtained from MeCN. ^{1}H NMR (CD_2Cl_2, 300 MHz): δ 8.29 (ddd, 2H, pyH-*o*), 7.02 (m, 2H, pyH-*m*), 6.80 (ddd, J = 5.6, 1.5, 0.6 Hz, 2H, pyH-*m*), 2.28 (s, 6H, CH_3) ppm. ^{13}C NMR (CD_2Cl_2, 75 MHz): δ 166.15 (s, 2C, C_q), 153.24 (s, 2C, C_q), 145.00 (s, 2C, pyC-*o*), 126.50 (s, 2C, pyC-*m*), 121.63 (s, 2C, pyC-*m*), 21.86 (s, 2C, CH_3) ppm. IR (cm^{-1}): 2955 (w), 2922 (w), 2852 (w), 1591 (s), 1539 (m), 1462 (m), 1435 (m), 1383 (s), 1271 (s), 1127 (m), 1092 (m), 1012 (m), 922 (s, Mo═O), 894 (s, Mo═O), 873 (s), 819 (s), 725 (m), 554 (w), 540 (m), 457 (m), 431 (m). EI-MS (70 eV) m/z: M^+ 378.0. Anal. Calcd for $C_{12}H_{12}N_2O_2S_2Mo$: C, 38.30; H, 3.21; N, 7.44; S, 17.04. Found: C, 38.05; H, 3.12; N, 7.50; S, 16.64.

*[MoO$_2$(6-MePyS)$_2$] (**4**).* Na(6-MePyS) (883 mg, 6.00 mmol) was added portionwise to a stirred solution of $MoO_2Cl_2(DMF)_2$ (1.04 g, 3.00 mmol) in 30 mL of MeCN. After 20 min, the solvent was evaporated *in vacuo*. The solid was then extracted with 100 mL of toluene, and the resulting suspension was filtered through Celite, yielding an orange solution. The solvent was evaporated, and the resulting solid was washed with 10 mL of MeCN and finally dried *in vacuo* to give [MoO_2(6-MePyS)$_2$](856 mg, 76%) as an orange microcrystalline powder. Single crystals suitable for X-ray diffraction analysis were obtained from CH_2Cl_2/heptane at −35 °C. ^{1}H NMR (CD_2Cl_2, 300 MHz): δ 7.51 (t, J = 7.8 Hz, 2H, pyH-*p*), 7.03 (d, J =

https://dx.doi.org/10.1021/acs.inorgchem.0c02412
Inorg. Chem. XXXX, XXX, XXX−XXX

7.8 Hz, 2H, pyH-*m*), 6.85 (d, *J* = 7.8 Hz, 2H, pyH-*m*), 2.65 (s, 6H, CH_3) ppm. ^{13}C NMR (CD_2Cl_2, 75 MHz): δ 166.71 (s, 2C, pyC-*o*), 158.77 (s, 2C, pyC-*o*), 139.98 (s, 2C, pyC-*p*), 122.95 (s, 2C, pyC-*m*), 121.21 (s, 2C, pyC-*m*), 24.44 (s, 2C, CH_3) ppm. IR (cm^{-1}): 1585 (m), 1557 (m), 1548 (m), 1440 (s), 1372 (m), 1172 (s), 1011 (w), 928 (s, Mo═O), 896 (s, Mo═O), 876 (m), 774 (s), 727 (m), 685 (m), 555 (w), 462 (m). EI-MS (70 eV) *m/z*: M^+ 378.1. Anal. Calcd for $C_{12}H_{12}N_2O_2S_2Mo$: C, 38.30; H, 3.21; N, 7.44; S, 17.04. Found: C, 38.36; H, 3.35; N, 7.49; S, 16.69.

*[$Mo_2O_3L_4$] (**6**−**9**).* PPh_3 (79 mg, 0.30 mmol) was added to a suspension of [MoO_2L_2] (**1**−**4**) (0.50 mmol) in 10 mL of MeCN. The mixture was stirred for 2 h, and the volume of the reaction mixture was reduced by half before 5 mL of Et_2O was added. The dark precipitate was isolated by filtration, washed with 3 mL of Et_2O, and dried *in vacuo*.

*[Mo_2O_3(PymS)$_4$] (**6**).* Yield: 159 mg (93%). IR (cm^{-1}): 1567 (m), 1542 (m), 1428 (m), 1366 (s), 1248 (m), 1185 (m), 1173 (m), 1162 (m), 1099 (w), 1067 (w), 947 (s, Mo═O), 822 (w), 810 (m), 798 (m), 762 (m), 746 (m), 662 (m), 653 (m), 468 (m), 438 (m, Mo−O−Mo). EI-MS (70 eV) *m/z*: [MoO_2(PymS)$_2$]$^+$ 351.9, [MoO(PymS)$_2$]$^+$ 335.9.

*[Mo_2O_3(PyS)$_4$] (**7**).* Yield: 154 mg (91%). IR (cm^{-1}): 1579 (s), 1549 (m), 1439 (m), 1417 (s), 1262 (m), 1132 (m), 941 (s, Mo═O), 878 (m), 775 (vw), 752 (s), 726 (s), 651 (m), 643 (m), 539 (w), 481 (m), 457 (m), 437 (m, Mo−O−Mo). EI-MS (70 eV) *m/z*: [MoO_2(PyS)$_2$]$^+$ 349.9, [MoO(PyS)$_2$]$^+$ 333.9.

*[Mo_2O_3(4-MePyS)$_4$] (**8**).* Yield: 182 mg (99%). IR (cm^{-1}): 1595 (s), 1539 (w), 1379 (m), 1268 (m), 1089 (m), 943 (s, Mo═O), 902 (w), 872 (m), 810 (m), 784 (m), 725 (m), 696 (w), 554 (m), 541 (m), 455 (m), 441 (s, Mo−O−Mo), 428 (m). EI-MS (70 eV) *m/z*: [MoO_2(4-MePyS)$_2$]$^+$ 378.0, [MoO(4-MePyS)$_2$]$^+$ 362.0. Anal. Calcd for $C_{24}H_{24}N_4O_3S_4Mo_2$: C, 39.13; H, 3.28; N, 7.61; S, 17.41. Found: C, 39.52; H, 3.17; N, 7.92; S, 15.92.

*[Mo_2O_3(6-MePyS)$_4$] (**9**).* Yield: 184 mg (100%). IR (cm^{-1}): 1582 (m), 1555 (m), 1447 (s), 1430 (s), 1171 (s), 930 (s, Mo═O), 877 (m), 777 (s), 729 (m), 692 (m), 683 (m), 563 (w), 542 (w), 464 (m), 436 (m, Mo−O−Mo). EI-MS (70 eV) *m/z*: [MoO_2(6-MePyS)$_2$]$^+$ 378.0, [MoO(6-MePyS)$_2$]$^+$ 362.0. Anal. Calcd for $C_{24}H_{24}N_4O_3S_4Mo_2$: C, 39.13; H, 3.28; N, 7.61; S, 17.41. Found: C, 39.58; H, 2.95; N, 7.44; S, 17.39.

*[MoO(PymS)$_2$(PMe$_3$)$_2$] (**10**).* A solution of PMe_3 (0.36 mL, 3.50 mmol) in 3 mL of MeCN was added to a stirred suspension of complex **4** (245 mg, 0.70 mmol) in 6 mL of MeCN. After 2 h, the volume of the deep orange-brown solution was reduced to approximately 3 mL. The resulting precipitate was isolated by filtration, washed with MeCN (2 × 2 mL), and subsequently dried *in vacuo* to give [MoO(PymS)$_2$(PMe$_3$)$_2$] (280 mg, 82%) as a dark brown crystalline powder. ^1H NMR (CD_2Cl_2, 300 MHz): δ 8.56 (d, *J* = 3.0 Hz, 4H, pymH-*o*), 6.66 (t, *J* = 5.1 Hz, 2H, pymH-*m*), 1.25 (t, $^2J_{HP}$ = 7.8 Hz, 18H, PCH_3) ppm. ^{13}C NMR (CD_2Cl_2, 75 MHz): δ 176.72 (m, 2C, Cq), 155.50 (bs, 4C, pymC-*o*), 113.40 (s, 2C, pymC-*m*), 14.61 (t, $^1J_{CP}$ = 24.6 Hz, 6C, PCH_3) ppm. ^{31}P NMR (CD_2Cl_2, 121 MHz): δ −9.00 ppm. IR (cm^{-1}): 2971 (w), 2903 (w), 1548 (w), 1532 (m), 1415 (m), 1361 (s), 1282 (m), 1246 (m), 1160 (m), 1086 (m), 1003 (m), 940 (s, Mo═O), 887 (m), 871 (s), 846 (m), 803 (m), 761 (m), 732 (m), 667 (w), 653 (m), 501 (w), 472 (m). EI-MS (70 eV) *m/z*: [M − 2 PMe_3]$^+$ 335.9. Anal. Calcd for $C_{14}H_{24}N_4OP_2S_2Mo$: C, 34.57; H, 4.97; N, 11.52; S, 13.18. Found: C, 34.51; H, 4.68; N, 11.76; S, 13.02.

*[MoO(PyS)$_2$(PMe$_3$)$_2$] (**11**).* A solution of PMe_3 (0.36 mL, 3.50 mmol) in 3 mL of CH_2Cl_2 was added to a stirred solution of **1** (244 mg, 0.70 mmol) in 6 mL of CH_2Cl_2. After 3 h, the solvent was evaporated. The resulting green solid was washed with MeCN (2 × 3 mL) and subsequently dried *in vacuo* to give [MoO(PyS)$_2$(PMe$_3$)$_2$] (281 mg, 83%) as a dark green microcrystalline powder. Single crystals suitable for X-ray diffraction analysis were obtained from MeCN. ^1H NMR (CD_2Cl_2, 300 MHz): δ 8.73 (ddd, *J* = 5.6, 0.7 Hz, 2H, pyH-*o*), 7.16 (td, *J* = 7.7, 1.7 Hz, 2H, pyH-*p*), 6.63 (ddd, *J* = 7.1, 5.6, 1.2 Hz, 2H, pyH-*m*), 6.56 (dt, *J* = 8.0, 1.0 Hz, 2H, pyH-*m*), 1.24 (t, $^2J_{HP}$ = 7.7 Hz, 18H, PCH_3) ppm. ^{13}C NMR (CD_2Cl_2, 75 MHz): δ 170.43 (s, 2C, C_q), 144.97 (s, 2C, pyC-*o*), 136.07 (s, 2C, pyC-*p*), 123.67 (s, 2C, pyC-*m*), 115.18 (s, 2C, pyC-*m*), 14.52 (t, $^1J_{CP}$ = 23.9 Hz, 6C, PCH_3) ppm. ^{31}P NMR (CD_2Cl_2, 121 MHz): δ −8.07 ppm. IR (cm^{-1}): 3071 (w), 3049 (w), 3027 (w), 2970 (w), 2900 (w), 1571 (m), 1540 (m), 1438 (m), 1416 (m), 1279 (m), 1248 (m), 1139 (m), 1085 (m), 937 (s, Mo═O), 876 (s), 847 (m), 758 (m), 747 (s), 734 (s), 666 (m), 504 (m), 469 (m). EI-MS (70 eV) *m/z*: [M − 2 PMe_3]$^+$3 34.0. Anal. Calcd for $C_{16}H_{26}N_2OP_2S_2Mo$: C, 39.67; H, 5.41; N, 5.78; S, 13.24. Found: C, 39.51; H, 5.14; N, 5.76; S, 12.99.

*[MoO(4-MePyS)$_2$(PMe$_3$)$_2$] (**12**).* A solution of PMe_3 (0.36 mL, 3.50 mmol) in 3 mL of MeCN was added to a stirred solution of **2** (263 mg, 0.70 mmol) in 4 mL of CH_2Cl_2 and 2 mL of MeCN. After 3 h, the volume of the now deep green solution was reduced to approximately 3 mL. The resulting precipitate was isolated by filtration, washed with 3 mL of MeCN, and subsequently dried *in vacuo* to give [MoO(4-MePyS)$_2$(PMe$_3$)$_2$] (359 mg, 100%) as a green microcrystalline powder. Single crystals suitable for X-ray diffraction analysis were obtained from CH_2Cl_2/heptane at −37 °C. ^1H NMR (CD_2Cl_2, 300 MHz): δ 8.55 (d, *J* = 5.7 Hz, 2H, pyH-*o*), 6.49 (dd, *J* = 5.7, 1.1 Hz, 2H, pyH-*m*), 6.44 (m, 2H, pyH-*m*), 2.24 (s, 6H, CH_3), 1.23 (t, $^2J_{HP}$ = 7.6 Hz, 18H, PCH_3) ppm. ^{13}C NMR (CD_2Cl_2, 75 MHz): δ 169.74 (s, 2C, SC_q), 147.53 (s, 2C, C_q), 144.39 (s, 2C, pyC-*o*), 124.17 (s, 2C, pyC-*m*), 117.10 (s, 2C, pyC-*m*), 20.98 (s, 2C, CH_3), 14.59 (t, $^1J_{CP}$ = 23.6 Hz, 6C, PCH_3) ppm. ^{31}P NMR (CD_2Cl_2, 121 MHz): δ − 7.86 ppm. IR (cm^{-1}): 3068 (w), 3048 (w), 3012 (w), 2970 (w), 2901 (w), 1588 (m), 1530 (m), 1454 (m), 1412 (m), 1375 (m), 1279 (m), 1223 (m), 1086 (m), 1007 (m), 941 (s, Mo═O), 885 (s), 873 (s), 846 (m), 813 (s), 730 (m), 700 (w), 668 (m), 563 (w), 472 (m), 444 (m). EI-MS (70 eV) *m/z*: [M − 2 PMe_3]$^+$ 362.0. Anal. Calcd for $C_{18}H_{30}N_2OP_2S_2Mo$: C, 42.19; H, 5.90; N, 5.47; S, 12.51. Found: C, 42.38; H, 5.75; N, 5.40; S, 11.84.

*[MoO(6-MePyS)$_2$(PMe$_3$)] (**13**).* A solution of PMe_3 (134 μL, 1.30 mmol) in 2 mL of CH_2Cl_2 was added to a stirred solution of **3** (188 mg, 0.50 mmol) in 8 mL of CH_2Cl_2. After 1 h, the solvent was evaporated *in vacuo*. The resulting green solid was first washed with 3 mL of MeCN and then recrystallized from CH_2Cl_2/heptane. After filtration and drying *in vacuo*, [MoO(6-MePyS)$_2$(PMe$_3$)] (192 mg, 88%) was obtained as a deep blue-green powder. ^1H NMR (CD_2Cl_2, 300 MHz): δ 7.50 (t, *J* = 7.8 Hz, 1H, pyH-*p*), 7.02−6.96 (m, 2H, pyH), 6.77−6.74 (m, 2H, pyH), 6.51 (d, *J* = 7.9 Hz, 1H, pyH-*m*), 2.79 (s, 3H, CH_3), 2.06 (s, 3H, CH_3), 1.46 (d, $^2J_{HP}$ = 9.0 Hz, 9H, PCH_3) ppm. ^{13}C NMR (CD_2Cl_2, 75 MHz): δ 183.16 (d, pyC-*o*), 169.21 (d, pyC-*o*), 159.83 (s, pyC-*o*), 158.96 (s, pyC-*o*), 140.28 (s, pyC-*p*), 134.35 (s, pyC-*p*), 125.09 (d, $^4J_{PC}$ = 1.7 Hz, pyC-*m*), 123.43 (s, pyC-*m*), 117.98 (s, pyC-*m*), 117.81 (d, $^4J_{PC}$ = 1.2 Hz, pyC-*m*), 25.14 (s, CH_3), 22.66 (s, CH_3), 16.14 (d, 3C, $^1J_{PC}$ = 27.6 Hz, PCH_3). ^{31}P NMR (CD_2Cl_2, 121 MHz): δ 8.23 ppm. IR (cm^{-1}): 3057 (w), 2980 (w), 2955 (w), 2907 (w), 1585 (m), 1578 (m), 1555 (m), 1540 (m), 1438 (m), 1422 (m), 1374 (m), 1300 (w), 1280 (m), 1236 (w), 1168 (m), 1086 (w), 937 (s, Mo═O), 875 (w), 843 (w), 793 (m), 777 (m), 729 (m), 685 (m), 668 (m), 558 (w), 467 (w). EI-MS (70 eV) *m/z*: [M − PMe_3]$^+$ 362.1. Anal. Calcd for $C_{15}H_{21}N_2OPS_2Mo$: C, 41.29; H, 4.85; N, 6.42; S, 14.69. Found: C, 41.16; H, 4.89; N, 6.60; S, 14.35.

X-ray Diffraction Analysis. Single-crystal X-ray diffraction analyses were carried out on a Bruker AXS SMART APEX-II diffractometer equipped with a CCD detector. All measurements were performed using monochromatized Mo K*α* radiation from an Incoatec microfocus sealed tube at 100 K. Absorption corrections were performed semiempirically from equivalents. Molecular structures were solved by direct methods (SHELXS-97)[108] and refined by full-matrix least-squares techniques against F^2 (SHELXL-2014/6).[109] Crystallographic data, figures, and selected geometry parameters are given in the Supporting Information. CCDC 1998303−1998313 and 2022748 contain supplementary crystallographic data for this paper. These data can be obtained free of charge via www.ccdc.cam.ac.uk/data_request/cif.

Catalytic Reactions. All catalytic experiments were performed at least three times under a nitrogen atmosphere in J. Young NMR tubes

https://dx.doi.org/10.1021/acs.inorgchem.0c02412
Inorg. Chem. XXXX, XXX, XXX−XXX

at 20−22 °C. All manipulations were carried out in a glovebox. In control experiments using Me_2SO, Ph_2SO, or $[Bu_4N][NO_3]$ and PPh_3 or PMe_3 without a metal complex under identical conditions, no conversion of the phosphine to the respective phosphine oxide was observed.

UV−Vis Spectroscopy. UV−vis spectra were recorded on a Varian Cary 50 spectrophotometer equipped with a VWR thermostat to control the temperatures of the kinetic studies using the Varian Cary WinUV software. The kinetic studies were performed at 25 °C in quartz cuvettes (d = 10 mm), and reaction solutions contained 0.1 mM of complex **1**, **2**, **3**, or **4** and 50, 100, and 150 equiv of PPh_3 in dry MeCN. Solutions were freshly prepared on the day of the experiments. After the reactions were scanned in the range λ = 600−300 nm, the progress of the OAT from complexes **1**−**4** to PPh_3 was followed by monitoring the change in absorbance at λ_{max} of the reaction product to determine the pseudo-first-order rate constants. Second-order rate constants k_2 were determined from the slope of the linear regression plots of k_{obs} versus $[PPh_3]$. Each experiment to determine k_{obs} at a certain PPh_3 concentration was independently performed at least three times.

DFT Calculations. All computations were performed using the TURBOMOLE 7.3 software package.[110] Structure optimizations were carried out without symmetry restraints utilizing the B3LYP[111−115]-D3[116] hybrid functional with a def2-TZVPPD basis set.[117,118] Thermochemical effects have been calculated with the rigid rotor harmonic oscillator approximation (RRHO) at 298 K. Instead of the much larger PPh_3, PMe_3 was used within the calculations.

■ ASSOCIATED CONTENT

Supporting Information

The Supporting Information is available free of charge at https://pubs.acs.org/doi/10.1021/acs.inorgchem.0c02412.

Full X-ray data, NMR spectra, and UV−vis data (PDF)

Accession Codes

CCDC 1998303−1998313 and 2022748 contain the supplementary crystallographic data for this paper. These data can be obtained free of charge via www.ccdc.cam.ac.uk/data_request/cif, or by emailing data_request@ccdc.cam.ac.uk, or by contacting The Cambridge Crystallographic Data Centre, 12 Union Road, Cambridge CB2 1EZ, UK; fax: +44 1223 336033.

■ AUTHOR INFORMATION

Corresponding Author

Nadia C. Mösch-Zanetti − *Institute of Chemistry, Inorganic Chemistry, University of Graz, 8010 Graz, Austria;* orcid.org/0000-0002-1349-6725; Email: nadia.moesch@uni-graz.at

Authors

Madeleine A. Ehweiner − *Institute of Chemistry, Inorganic Chemistry, University of Graz, 8010 Graz, Austria*

Fabian Wiedemaier − *Institute of Chemistry, Physical and Theoretical Chemistry, University of Graz, 8010 Graz, Austria*

Ferdinand Belaj − *Institute of Chemistry, Inorganic Chemistry, University of Graz, 8010 Graz, Austria*

Complete contact information is available at: https://pubs.acs.org/10.1021/acs.inorgchem.0c02412

Author Contributions

The manuscript was written through contributions of all authors. All authors have given approval to the final version of the manuscript.

Notes

The authors declare no competing financial interest.

■ ACKNOWLEDGMENTS

We especially wish to thank A. Daniel Boese for the permission to utilize his computational resources and Bernd Werner for measuring countless NMR samples. Financial support by NAWI Graz is also gratefully acknowledged.

■ REFERENCES

(1) Molybdenum and Tungsten Enzymes. In *Bioinorganic Chemistry*, 1st ed.; Hille, R., Schulzke, C., Kirk, M. L., Eds.; Royal Society of Chemistry: Cambridge, 2017; Metallobiology 6.

(2) Hille, R.; Hall, J.; Basu, P. The mononuclear molybdenum enzymes. *Chem. Rev.* **2014**, *114*, 3963−4038.

(3) Hille, R. Molybdenum and tungsten in biology. *Trends Biochem. Sci.* **2002**, *27*, 360−367.

(4) Basu, P.; Burgmayer, S. J. N. Pterin chemistry and its relationship to the molybdenum cofactor. *Coord. Chem. Rev.* **2011**, *255*, 1016−1038.

(5) Pushie, M. J.; Cotelesage, J. J.; George, G. N. Molybdenum and tungsten oxygen transferases—and functional diversity within a common active site motif. *Metallomics* **2014**, *6*, 15−24.

(6) Leimkühler, S.; Wuebbens, M. M.; Rajagopalan, K. V. The History of the Discovery of the Molybdenum Cofactor and Novel Aspects of its Biosynthesis in Bacteria. *Coord. Chem. Rev.* **2011**, *255*, 1129−1144.

(7) Hille, R. The molybdenum oxotransferases and related enzymes. *Dalton Trans.* **2013**, *42*, 3029−3042.

(8) Magalon, A.; Fedor, J. G.; Walburger, A.; Weiner, J. H. Molybdenum enzymes in bacteria and their maturation. *Coord. Chem. Rev.* **2011**, *255*, 1159−1178.

(9) Kisker, C.; Schindelin, H.; Baas, D.; Rétey, J.; Meckenstock, R. U.; Kroneck, P. M. H. A structural comparison of molybdenum cofactor-containing enzymes. *FEMS Microbiol. Rev.* **1998**, *22*, 503−521.

(10) Youngblut, M. D.; Tsai, C.-L.; Clark, I. C.; Carlson, H. K.; Maglaqui, A. P.; Gau-Pan, P. S.; Redford, S. A.; Wong, A.; Tainer, J. A.; Coates, J. D. Perchlorate Reductase Is Distinguished by Active Site Aromatic Gate Residues. *J. Biol. Chem.* **2016**, *291*, 9190−9202.

(11) Sun, S.-Q.; Chen, S.-L. How does Mo-dependent perchlorate reductase work in the decomposition of oxyanions? *Dalton Trans.* **2019**, *48*, 5683−5691.

(12) Young, C. G.; Wedd, A. G. Metal chemistry relevant to the mononuclear molybdenum and tungsten pterin enzymes. *Chem. Commun.* **1997**, 1251−1257.

(13) Sengar, R. S.; Basu, P. Design, Syntheses, and Characterization of a Sterically Encumbered Dioxo Molybdenum(VI) Core. *Inorg. Chim. Acta* **2007**, *360*, 2092−2099.

(14) Millar, A. J.; Doonan, C. J.; Smith, P. D.; Nemykin, V. N.; Basu, P.; Young, C. G. Oxygen atom transfer in models for molybdenum enzymes: isolation and structural, spectroscopic, and computational studies of intermediates in oxygen atom transfer from molybdenum(VI) to phosphorus(III). *Chem. - Eur. J.* **2005**, *11*, 3255−3267.

(15) Oku, H.; Ueyama, N.; Kondo, M.; Nakamura, A. Oxygen atom transfer systems in which the μ-oxodimolybdenum(V) complex formation does not occur: syntheses, structures, and reactivities of monooxomolybdenum(IV) benzenedithiolato complexes as models of molybdenum oxidoreductases. *Inorg. Chem.* **1994**, *33*, 209−216.

(16) Ghosh, A. C.; Samuel, P. P.; Schulzke, C. Synthesis, characterization and oxygen atom transfer reactivity of a pair of Mo(IV)O- and Mo(VI)O_2-enedithiolate complexes - a look at both ends of the catalytic transformation. *Dalton Trans.* **2017**, *46*, 7523−7533.

(17) Arzoumanian, H. Molybdenum-oxo chemistry in various aspects of oxygen atom transfer processes. *Coord. Chem. Rev.* **1998**, *178−180*, 191−202.

(18) Basu, P.; Nemykin, V. N.; Sengar, R. S. Substituent effect on oxygen atom transfer reactivity from oxomolybdenum centers: synthesis, structure, electrochemistry, and mechanism. *Inorg. Chem.* **2009**, *48*, 6303−6313.

(19) Enemark, J. H.; Cooney, J. J. A.; Wang, J.-J.; Holm, R. H. Synthetic analogues and reaction systems relevant to the molybdenum and tungsten oxotransferases. *Chem. Rev.* **2004**, *104*, 1175−1200.
(20) Reynolds, M. S.; Berg, J. M.; Holm, R. H. Kinetics of oxygen atom transfer reactions involving oxomolybdenum complexes. General treatment for reactions with intermediate oxo-bridged molybdenum(V) dimer formation. *Inorg. Chem.* **1984**, *23*, 3057−3062.
(21) Holm, R. H. Metal-Centered Oxygen Atom Transfer Reactions. *Chem. Rev.* **1987**, *87*, 1401−1449.
(22) Berg, J. M.; Holm, R. H. Model for the active sites of oxo-transfer molybdoenzymes: reactivity, kinetics, and catalysis. *J. Am. Chem. Soc.* **1985**, *107*, 925−932.
(23) Majumdar, A.; Sarkar, S. Bioinorganic chemistry of molybdenum and tungsten enzymes: A structural−functional modeling approach. *Coord. Chem. Rev.* **2011**, *255*, 1039−1054.
(24) Majumdar, A. Structural and functional models in molybdenum and tungsten bioinorganic chemistry: description of selected model complexes, present scenario and possible future scopes. *Dalton Trans.* **2014**, *43*, 8990−9003.
(25) Volpe, M.; Mösch-Zanetti, N. C. Molybdenum(VI) dioxo and oxo-imido complexes of fluorinated β-ketiminato ligands and their use in OAT reactions. *Inorg. Chem.* **2012**, *51*, 1440−1449.
(26) Schultz, B. E.; Hille, R.; Holm, R. H. Direct oxygen atom transfer in the mechanism of action of Rhodobacter sphaeroides dimethyl sulfoxide reductase. *J. Am. Chem. Soc.* **1995**, *117*, 827−828.
(27) Randolph, A. H.; Seewald, N. J.; Rickert, K.; Brown, A. S. N. Tris(3,5-di-tert-butylcatecholato)molybdenum(VI): Lewis acidity and nonclassical oxygen atom transfer reactions. *Inorg. Chem.* **2013**, *52*, 12587−12598.
(28) Paul, T.; Rodehutskors, P. M.; Schmidt, J.; Burzlaff, N. Oxygen Atom Transfer Catalysis with Homogenous and Polymer-Supported N, N- and N, N, O-Heteroscorpionate Dioxidomolybdenum(VI) Complexes. *Eur. J. Inorg. Chem.* **2016**, *2016*, 2595−2602.
(29) Hüttinger, K.; Förster, C.; Bund, T.; Hinderberger, D.; Heinze, K. Stereochemical consequences of oxygen atom transfer and electron transfer in imido/oxido molybdenum(IV, V, VI) complexes with two unsymmetric bidentate ligands. *Inorg. Chem.* **2012**, *51*, 4180−4192.
(30) Schultz, B. E.; Gheller, S. F.; Muetterties, M. C.; Scott, M. J.; Holm, R. H. Molybdenum-Mediated Oxygen Atom Transfer: An Improved Analogue Reaction System of the Molybdenum Oxo-transferases. *J. Am. Chem. Soc.* **1993**, *115*, 2714.
(31) Oheix, E.; Orio, M.; Giorgi, M.; Réglier, M.; Iranzo, O.; Hardré, R. Y. An Air-Stable Molybdenum-Based Precatalyst in Oxygen-Atom Transfer Reactions. *Eur. J. Inorg. Chem.* **2018**, *2018*, 1427−1434.
(32) Chrysochos, N.; Ahmadi, M.; Wahlefeld, S.; Rippers, Y.; Zebger, I.; Mroginski, M. A.; Schulzke, C. Comparison of molybdenum and rhenium oxo bis-pyrazine-dithiolene complexes - in search of an alternative metal centre for molybdenum cofactor models. *Dalton Trans.* **2019**, *48*, 2701−2714.
(33) Schindler, T.; Sauer, A.; Spaniol, T. P.; Okuda, J. Oxygen Atom Transfer Reactions with Molybdenum Cofactor Model Complexes That Contain a Tetradentate OSSO-Type Bis(phenolato) Ligand. *Organometallics* **2018**, *37*, 4336−4340.
(34) Saswati; Roy, S.; Dash, S. P.; Acharyya, R.; Kaminsky, W.; Ugone, V.; Garribba, E.; Harris, C.; Lowe, J. M.; Dinda, R. Chemistry of oxidomolybdenum(IV) and -(VI) complexes with ONS donor ligands. *Polyhedron* **2018**, *141*, 322−336.
(35) Maurya, M. R.; Uprety, B.; Avecilla, F. Dioxidomolybdenum(VI) Complexes of Tripodal Tetradentate Ligands for Catalytic Oxygen Atom Transfer between Benzoin and Dimethyl Sulfoxide and for Oxidation of Pyrogallol. *Eur. J. Inorg. Chem.* **2016**, *2016*, 4802−4813.
(36) Maurya, M. R.; Mengesha, B.; Uprety, B.; Jangra, N.; Tomar, R.; Avecilla, F. Oxygen atom transfer between DMSO and benzoin catalyzed by cis -dioxidomolybdenum(vi) complexes of tetradentate Mannich bases. *New J. Chem.* **2018**, *42*, 6225−6235.
(37) Khatua, S.; Naskar, T.; Nandi, C.; Majumdar, A. Mononuclear bis(dithiolene) Mo(IV) and W(IV) complexes with P, P; S, S; O, S and O, O donor ligands: a comparative reactivity study. *New J. Chem.* **2017**, *41*, 9769−9783.
(38) Ducrot, A. B.; Coulson, B. A.; Perutz, R. N.; Duhme-Klair, A.-K. Light-Induced Activation of a Molybdenum Oxotransferase Model within a Ru(II)-Mo(VI) Dyad. *Inorg. Chem.* **2016**, *55*, 12583−12594.
(39) Ducrot, A.; Scattergood, B.; Coulson, B.; Perutz, R. N.; Duhme-Klair, A.-K. Electronic Fine-Tuning of Oxygen Atom Transfer Reactivity of cis-Dioxomolybdenum(VI) Complexes with Thiosemicarbazone Ligands. *Eur. J. Inorg. Chem.* **2015**, *2015*, 3562−3571.
(40) Arumuganathan, T.; Mayilmurugan, R.; Volpe, M.; Mösch-Zanetti, N. C. Faster oxygen atom transfer catalysis with a tungsten dioxo complex than with its molybdenum analog. *Dalton Trans.* **2011**, *40*, 7850−7857.
(41) Tran, B. L.; Carrano, C. J. Oxo-molybdenum(VI, V, IV) complexes of the facially coordinating tris(mercaptoimidazolyl)borate ligand: synthesis, characterization, and oxygen atom transfer reactivity. *Inorg. Chem.* **2007**, *46*, 5429−5438.
(42) Tran, B. L.; Arita, A.; Cooksy, A. L.; Carrano, C. J. Examination of oxygen atom transfer reactivity of heteroscorpionate dioxo-Mo(VI) complexes: Geometric isomers, solvent effect, intermediates, and catalytic oxidation. *Inorg. Chim. Acta* **2016**, *447*, 45−51.
(43) Smith, P. D.; Millar, A. J.; Young, C. G.; Ghosh, A.; Basu, P. Detection, Isolation, and Characterization of Intermediates in Oxygen Atom Transfer Reactions in Molybdoenzyme Model Systems. *J. Am. Chem. Soc.* **2000**, *122*, 9298−9299.
(44) Sengar, R. S.; Nemykin, V. N.; Basu, P. Synthesis, electrochemistry, geometric and electronic structure of oxo-molybdenum compounds involved in an oxygen atom transferring system. *J. Inorg. Biochem.* **2008**, *102*, 748−756.
(45) Roberts, S. A.; Young, C. G.; Kipke, C. A.; Cleland, W. E., Jr; Yamanouchi, K.; Carducci, M. D.; Enemark, J. H. Dioxomolybdenum(VI) complexes of the hydrotris(3,5-dimethyl-1-pyrazolyl)borate ligand. Synthesis and oxygen atom transfer reactions. *Inorg. Chem.* **1990**, *29*, 3650−3656.
(46) Roberts, S. A.; Young, C. G.; Cleland, W. E., Jr; Ortega, R. B.; Enemark, J. H. Synthesis, characterization, and oxygen atom transfer reactions of $\{HB(Me_2C_3N_2H)_3\}MoO\{S_2P(OR)_2\}$ and $\{HB(Me_2C_3N_2H)_3\}MoO_2\{\eta^1\text{-}S_2P(OEt)_2\}$. *Inorg. Chem.* **1988**, *27*, 3044−3051.
(47) Nemykin, V. N.; Basu, P. Oxygen atom transfer reactivity from a dioxo-Mo(VI) complex to tertiary phosphines: synthesis, characterization, and structure of phosphoryl intermediate complexes. *Inorg. Chem.* **2005**, *44*, 7494−7502.
(48) Young, C. G. Scorpionate Complexes as Models for Molybdenum Enzymes. *Eur. J. Inorg. Chem.* **2016**, *2016*, 2357−2376.
(49) Dong, G.; Ryde, U. Effect of the protein ligand in DMSO reductase studied by computational methods. *J. Inorg. Biochem.* **2017**, *171*, 45−51.
(50) Ryde, U.; Schulzke, C.; Starke, K. Which functional groups of the molybdopterin ligand should be considered when modeling the active sites of the molybdenum and tungsten cofactors? A density functional theory study. *JBIC, J. Biol. Inorg. Chem.* **2009**, *14*, 1053−1064.
(51) Paudel, J.; Pokhrel, A.; Kirk, M. L.; Li, F. Remote Charge Effects on the Oxygen-Atom-Transfer Reactivity and Their Relationship to Molybdenum Enzymes. *Inorg. Chem.* **2019**, *58*, 2054−2068.
(52) Li, J.; Andrejić, M.; Mata, R. A.; Ryde, U. A Computational Comparison of Oxygen Atom Transfer Catalyzed by Dimethyl Sulfoxide Reductase with Mo and W. *Eur. J. Inorg. Chem.* **2015**, *2015*, 3580−3589.
(53) Li, J.; Ryde, U. Comparison of the active-site design of molybdenum oxo-transfer enzymes by quantum mechanical calculations. *Inorg. Chem.* **2014**, *53*, 11913−11924.
(54) Craig, J. A.; Holm, R. H. Reduction of nitrate to nitrite by molybdenum-mediated atom transfer. *J. Am. Chem. Soc.* **1989**, *111*, 2111−2115.
(55) Elrod, L. T.; Kim, E. Lewis Acid Assisted Nitrate Reduction with Biomimetic Molybdenum Oxotransferase Complex. *Inorg. Chem.* **2018**, *57*, 2594−2602.

https://dx.doi.org/10.1021/acs.inorgchem.0c02412
Inorg. Chem. XXXX, XXX, XXX−XXX

(56) Majumdar, A.; Pal, K.; Sarkar, S. Chemistry of $[Et_4N]$-$[Mo^{IV}(SPh)(PPh_3)(mnt)_2]$ as an analogue of dissimilatory nitrate reductase with its inactivation on substitution of thiolate by chloride. *J. Am. Chem. Soc.* **2006**, *128*, 4196−4197.
(57) Jiang, J.; Holm, R. H. Reaction Systems Related to Dissimilatory Nitrate Reductase. *Inorg. Chem.* **2005**, *44*, 1068−1072.
(58) Wick, K.; Heumesser, C.; Schmid, E. Groundwater nitrate contamination: factors and indicators. *J. Environ. Manage.* **2012**, *111*, 178−186.
(59) Almasri, M. N. Nitrate contamination of groundwater: A conceptual management framework. *Environ. Impact Assess. Rev.* **2007**, *27*, 220−242.
(60) Arnáiz, F. J.; Aguado, R.; Pedrosa, M. R.; Maestro, M. A. Dioxomolybdenum(VI) thionates. *Polyhedron* **2004**, *23*, 537−543.
(61) Traill, P. R.; Wedd, A. G.; Tiekink, E. R. T. Synthesis and structure of cis-dioxobis(pyrimidine-2-thiolato-N, S)molybdenum-(VI). *Aust. J. Chem.* **1992**, *45*, 1933−1937.
(62) Ma, X.; Schulzke, C.; Yang, Z.; Ringe, A.; Magull, J. Synthesis, structures and oxygen atom transfer catalysis of oxo-bridged molybdenum(V) complexes with heterocyclic bidentate ligands (N, X) X = S, Se. *Polyhedron* **2007**, *26*, 5497−5505.
(63) Moran, D.; Sukcharoenphon, K.; Puchta, R.; Schaefer, H. F.; Schleyer, P. v. R.; Hoff, C. D. 2-Pyridinethiol/2-Pyridinethione Tautomeric Equilibrium. A Comparative Experimental and Computational Study. *J. Org. Chem.* **2002**, *67*, 9061−9069.
(64) Miranda-Soto, V.; Pérez-Torrente, J. J.; Oro, L. A.; Lahoz, F. J.; Martín, M. L.; Parra-Hake, M.; Grotjahn, D. B. Effects of the Heterocycle and Its Substituents on Structure and Fluxionality in Rhodium(I) and Iridium(I) Complexes with the Hindered Thiolates 6-*tert*-Butylpyridine-2-thiolate and 1-Alkyl-4-*tert*-butylimidazole-2-thiolate (alkyl = methyl and *tert*-butyl). *Organometallics* **2006**, *25*, 4374−4390.
(65) Kanishchev, O. S.; Dolbier, W. R. Synthesis and Characterization of 2-Pyridylsulfur Pentafluorides. *Angew. Chem., Int. Ed.* **2015**, *54*, 280−284.
(66) Mayer, J. M. Metal-oxygen multiple bond lengths: a statistical study. *Inorg. Chem.* **1988**, *27*, 3899−3903.
(67) Cotton, F. A.; Ilsley, W. H. Preparation and Characterization of bis(2-thiopyrimidinato)bis(pyridine)-dioxodi(μ-oxo)dimolybdenum-(V). *Inorg. Chim. Acta* **1982**, *59*, 213−217.
(68) Hoffmann, P.; Mattes, R. Nitrosyl-, halogeno-, and oxomolybdenum complexes with the ligand 1-thia-4,7-diazacyclononane (L). *Inorg. Chem.* **1989**, *28*, 2092−2096.
(69) Kay, A.; Drew, M. G. B. Crystal and molecular strcture of di-y-oxo-bis[oxo(L-cysteinato ethyl ester-N, S)-molybdenum(V)]. *J. Chem. Soc. A* **1971**, *0*, 1846−1850.
(70) Mikuriya, M.; Kusunoki, K.; Kotera, T.; Yoshioka, D.; Ogasawara, K. Synthesis, Crystal Structure, and DFT Calculation of a Doxido-bridged Dinuclear Oxidomolybdenum(V) Complex with 2-(2-Aminoethyl)-aminoethanethiol. *X-Ray Struct. Anal. Online* **2017**, *33*, 37−39.
(71) Peschel, L. M.; Belaj, F.; Schachner, J. A.; Mösch-Zanetti, N. C. Dinuclear Mo^V Complexes with Thiophenolate-oxazoline Ligands. *Eur. J. Inorg. Chem.* **2017**, *2017*, 2808−2817.
(72) Zhang, Q.; Starke, K.; Schulzke, C.; Hofmeister, A.; Magull, J. Different reaction behaviour of molybdenum and tungsten − Reactions of the dichloro dioxo dimethyl-bispyridine complexes with thiophenolate. *Inorg. Chim. Acta* **2007**, *360*, 3400−3407.
(73) Dahlstrom, P. L.; Hyde, J. R.; Vella, P. A.; Zubieta, J. Investigations of the coordination chemistry of molybdenum with facultative tetradentate ligands possessing N_2S_2 donor sets. *Inorg. Chem.* **1982**, *21*, 927−932.
(74) Block, E..; Gernon, M..; Kang, H..; Ofori-Okai, G..; Zubieta, J.. Preparations, structures and reactions of molybdenum complexes of triorgano silylated pyridine-2-thiols. *Inorg. Chem.* **1991**, *30*, 1736−1747.
(75) Gupta, S.; Roy, S.; Mandal, T. N.; Das, K.; Ray, S.; Butcher, R. J.; Kar, S. K. Synthesis, characterization and spectrochemical studies on a few binuclear μ-oxo molybdenum(V) complxes of pyrimidine derived Schiff base ligands. *J. Chem. Sci.* **2010**, *122*, 239−245.
(76) Barnard, K. R.; Bruck, M.; Huber, S.; Grittini, C.; Enemark, J. H.; Gable, R. W.; Wedd, A. G. Mononuclear and Binuclear Molybdenum(V) Complexes of the Ligand N, N'-Dimethyl-N, N'-bis(2-mercaptophenyl)ethylenediamine: Geometric Isomers. *Inorg. Chem.* **1997**, *36*, 637−649.
(77) Cotton, F. A.; Hunter, D. L.; Ricard, L.; Weiss, R. The Infrared Spectra of some Mono- and Binuclear Oxo-complexes of Molybdenum(IV), -(V), and -(VI); The Assignment of $(LL)_4Mo_2O_3$ Spectra. *J. Coord. Chem.* **1974**, *3*, 259−261.
(78) Lincoln, S. E.; Loehr, T. M. Chemistry and electronic and vibrational spectroscopy of mononuclear and dinuclear (tris(1-pyrazolyl)borato)- and chloro molybdenum(V)-oxo complexes. *Inorg. Chem.* **1990**, *29*, 1907−1915.
(79) Topaloglu-Sozuer, I.; Irdem, S. D.; Jeffery, J. J.; Hamidov, H.; Senturk, O. S. Oxo-brridged (haloarylimido)[tris(3,4-dimethylpyrazolyl)borato]-molybdenum(V) complexes. *Z. Naturforsch., B: J. Chem. Sci.* **2005**, *60*, 15−21.
(80) Cotton, F. A.; Falvello, L. R.; Meadows, J. H. Structural characterization and infrared studies of tungsten bromo carbonyl compounds. *Inorg. Chem.* **1985**, *24*, 514−517.
(81) Tolman, C. A. Steric effects of phosphorus ligands in organometallic chemistry and homogeneous catalysis. *Chem. Rev.* **1977**, *77*, 313−348.
(82) Dupé, A.; Judmaier, M. E.; Belaj, F.; Zangger, K.; Mösch-Zanetti, N. C. Activation of molecular oxygen by a molybdenum complex for catalytic oxidation. *Dalton Trans.* **2015**, *44*, 20514−20522.
(83) Zwettler, N.; Judmaier, M. E.; Strohmeier, L.; Belaj, F.; Mösch-Zanetti, N. C. Oxygen activation and catalytic aerobic oxidation by Mo(IV)/(VI) complexes with functionalized iminophenolate ligands. *Dalton Trans.* **2016**, *45*, 14549−14560.
(84) Lyashenko, G.; Saischek, G.; Pal, A.; Herbst-Irmer, R.; Mösch-Zanetti, N. C. Molecular oxygen activation by a molybdenum(IV) monooxo bis(beta-ketiminato) complex. *Chem. Commun.* **2007**, No. 7, 701−703.
(85) Zwettler, N.; Ehweiner, M. A.; Schachner, J. A.; Dupé, A.; Belaj, F.; Mösch-Zanetti, N. C. Dioxygen Activation with Molybdenum Complexes Bearing Amide-Functionalized Iminophenolate Ligands. *Molecules* **2019**, *24*, 1814.
(86) Hanauer, K.; Förster, C.; Heinze, K. Redox-Controlled Stabilization of an Open-Shell Intermediate in a Bioinspired Enzyme Model. *Eur. J. Inorg. Chem.* **2018**, *2018*, 3537−3547.
(87) Jacobsen, N. E. NMR Spectroscopy Explained. *Simplified Theory, Applications and Examples for Organic Chemistry and Structural Biology*; Wiley: Hoboken, NJ, 2007.
(88) Atwood, J. L.; Hunter, W. E.; Carmona-Guzman, E.; Wilkinson, G. Synthesis and crystal structure of hydrido(tetrahydroborato)-tetrakis(trimethylphosphine)molybdenum(II). *J. Chem. Soc., Dalton Trans.* **1980**, *3*, 467−470.
(89) Hursthouse, M. B.; Lyons, D.; Thornton-Pett, M.; Wilkinson, G. Trimethylphosphine hydrides of molybdenum(II), tungsten(VI), and rhenium(VII): x-ray crystal structure of pentakis-(trimethylphosphine)dihydridomolybdenum(II). *J. Chem. Soc., Chem. Commun.* **1983**, *18*, 476−477.
(90) Carmona, E.; Sánchez, L.; Marin, J. M.; Povea, M. L.; Atwood, J. L.; Priester, R. D.; Rogers, R. D. η^2-acyl coordination and β-C-H interaction in acyl complexes of molybdenum. *J. Am. Chem. Soc.* **1984**, *106*, 3214−3222.
(91) Lyons, D.; Wilkinson, G.; Thornton-Pett, M.; Hursthouse, M. B. Synthesis, X-ray crystal structure, and reactions of dihydridopentakis(trimethylphosphine)molybdenum(II). *J. Chem. Soc., Dalton Trans.* **1984**, 695−700.
(92) Carmona, E.; Munoz, M. A.; Rogers, R. D. Synthesis, characterization, and properties of the η^2-acyl complexes $Mo(\eta^2$-$COCH_2CMe_3)X(PMe_3)_4$ (X = Cl, Br). *Inorg. Chem.* **1988**, *27*, 1598−1601.

https://dx.doi.org/10.1021/acs.inorgchem.0c02412
Inorg. Chem. XXXX, XXX, XXX−XXX

(93) Hascall, T.; Bridgewater, B. M.; Parkin, G. Reactivity of $Mo(PMe_3)_5H_2$ towards catecholborane. *Polyhedron* **2000**, *19*, 1063−1066.
(94) Zhu, G.; Tanski, J. M.; Parkin, G. Synthesis and structure of [pzBu2t]Mo(PMe3)4H, a d4 molybdenum complex that exhibits η^2-coordination of the 3,5-di-*t*-butylpyrazolyl ligand. *Polyhedron* **2003**, *22*, 199−203.
(95) Zhu, G.; Parkin, G. Synthesis and structural characterization of $M(PMe_3)_3(O_2CR)_2(OH_2)H_2$ (M = Mo, W). *Inorg. Chem.* **2005**, *44*, 9637−9639.
(96) Zhu, G.; Pang, K.; Parkin, G. New modes for coordination of aromatic heterocyclic nitrogen compounds to molybdenum: catalytic hydrogenation of quinoline, isoquinoline, and quinoxaline by $Mo(PMe_3)_4H_4$. *J. Am. Chem. Soc.* **2008**, *130*, 1564−1565.
(97) Zuzek, A. A.; Parkin, G. Si-H and Si-C bond cleavage reactions of silane and phenylsilanes with $Mo(PMe_3)_6$: silyl, hypervalent silyl, silane, and disilane complexes. *J. Am. Chem. Soc.* **2014**, *136*, 8177−8180.
(98) Holm, R. H. The biologically relevant oxygen atom transfer chemistry of molybdenum: From synthetic analogue systems to enzymes. *Coord. Chem. Rev.* **1990**, *100*, 183−221.
(99) Lim, M. D.; Lorkovic, I. M.; Ford, P. C. Kinetics of the oxidation of triphenylphosphine by nitric oxide. *Inorg. Chem.* **2002**, *41*, 1026−1028.
(100) Abernethy, R. J.; Foreman, M. R. S.-J.; Hill, A. F.; Tshabang, N.; Willis, A. C.; Young, R. D. Poly(methimazolyl)borato Nitrosyl Complexes of Molybdenum and Tungsten. *Organometallics* **2008**, *27*, 4455−4463.
(101) Campo, J. A.; Cano, M.; Heras, J. V.; Lagunas, M. C.; Pinilla, E.; Torres, M. R. Bowl-shaped molybdenum complexes containing tris(3-p-methoxyphenylpyrazol-1-yl)borate (TpAn). *Polyhedron* **2001**, *20*, 2997−3005.
(102) Yonemura, T. Nitrosyltris(pyridine-2-thiolato-κ-N, S)-molybdenum(II) dihydrate. *Acta Crystallogr., Sect. E: Struct. Rep. Online* **2009**, *65*, m1463−m1464.
(103) Nemykin, V. N.; Laskin, J.; Basu, P. Isolation, characterization of an intermediate in an oxygen atom-transfer reaction, and the determination of the bond dissociation energy. *J. Am. Chem. Soc.* **2004**, *126*, 8604−8605.
(104) Sanz, R.; Escribano, J.; Aguado, R.; Pedrosa, M.; Arnáiz, F. Selective Deoxygenation of Sulfoxides to Sulfides with Phosphites Catalyzed by Dichlorodioxomolybdenum(VI). *Synthesis* **2004**, *2004*, 1629−1632.
(105) Adger, B. M.; Ayrey, P.; Bannister, R.; Forth, M. A.; Hajikarimian, Y.; Lewis, N. J.; O'Farrell, C.; Owens, N.; Shamji, A. Synthesis of 2-substituted 4-pyridylpropionates. Part 2. Alkylation approach. *J. Chem. Soc., Perkin Trans. 1* **1988**, *10*, 2791−2796.
(106) Hintermann, L.; Dang, T. T.; Labonne, A.; Kribber, T.; Xiao, L.; Naumov, P. The AZARYPHOS family of ligands for ambifunctional catalysis: syntheses and use in ruthenium-catalyzed anti-Markovnikov hydration of terminal alkynes. *Chem. - Eur. J.* **2009**, *15*, 7167−7179.
(107) Cotton, F. A.; Fanwick, P. E.; Fitch, J. W.; Fitch, J. W. Two New Molybdenum Complexes and Their Structures. *Inorg. Chem.* **1978**, *17*, 3254−3257.
(108) Sheldrick, G. M. A short history of SHELX. *Acta Crystallogr., Sect. A: Found. Crystallogr.* **2008**, *64*, 112−122.
(109) Sheldrick, G. M. Crystal structure refinement with SHELXL. *Acta Crystallogr., Sect. C: Struct. Chem.* **2015**, *71*, 3−8.
(110) TURBOMOLE 7.3 [Online], available from http://www.turbomole.com.
(111) Becke, A. D. Density-functional exchange-energy approximation with correct asymptotic behavior. *Phys. Rev. A: At., Mol., Opt. Phys.* **1988**, *38*, 3098−3100.
(112) Becke, A. D. Density-functional thermochemistry. III. The role of exact exchange. *J. Chem. Phys.* **1993**, *98*, 5648−5652.
(113) Lee, C.; Yang, W.; Parr, R. G. Development of the Colle-Salvetti correlation-energy formula into a functional of the electron density. *Phys. Rev. B: Condens. Matter Mater. Phys.* **1988**, *37*, 785−789.
(114) Stephens, P. J.; Devlin, F. J.; Chabalowski, C. F.; Frisch, M. J. Ab Initio Calculation of Vibrational Absorption and Circular Dichroism Spectra Using Density Functional Force Fields. *J. Phys. Chem.* **1994**, *98*, 11623−11627.
(115) Vosko, S. H.; Wilk, L.; Nusair, M. Accurate spin-dependent electron liquid correlation energies for local spin density calculations: a critical analysis. *Can. J. Phys.* **1980**, *58*, 1200−1211.
(116) Grimme, S.; Antony, J.; Ehrlich, S.; Krieg, H. A consistent and accurate ab initio parametrization of density functional dispersion correction (DFT-D) for the 94 elements H-Pu. *J. Chem. Phys.* **2010**, *132*, 154104.
(117) Rappoport, D.; Furche, F. Property-optimized gaussian basis sets for molecular response calculations. *J. Chem. Phys.* **2010**, *133*, 134105.
(118) Weigend, F.; Furche, F.; Ahlrichs, R. Gaussian basis sets of quadruple zeta valence quality for atoms H−Kr. *J. Chem. Phys.* **2003**, *119*, 12753−12762.

https://dx.doi.org/10.1021/acs.inorgchem.0c02412
Inorg. Chem. XXXX, XXX, XXX−XXX